IEKP-KA/2016-25

Karlsruhe Institute of Technology

Determination of the Strong Coupling Constant from Inclusive Jet Data at the LHC, HERA and the Tevatron

Master's Thesis
of

Daniel Săvoiu

Department of Physics
Institut für Experimentelle
Kernphysik (IEKP)

Reviewer: Prof. Dr. Günter Quast
Second Reviewer: Prof. Dr. Wim de Boer

December 21, 2016

Ich versichere wahrheitsgemäß, die Arbeit selbstständig angefertigt, alle benutzten Hilfsmittel vollständig und genau angegeben und alles kenntlich gemacht zu haben, was aus Arbeiten anderer unverändert oder mit Abänderungen entnommen wurde.

Karlsruhe, den 21. Dezember 2016

. . . . . .

(**Daniel Săvoiu**)

Acknowledgements

My most sincere thanks go to Prof. Dr. Günter Quast for offering me the opportunity of researching such an interesting topic. His encouragement and insightful guidance have been invaluable.

I would also like to thank Prof. Dr. Wim de Boer for agreeing to be the second reviewer of this thesis.

To Dr. Klaus Rabbertz, who has supervised and supported the development of this thesis, I express my sincere gratitude for his attentive and dedicated support, as well as for the detailed insights he has offered during the entire course of this work.

I am much indebted to Dr. Georg Sieber for the expertise he has shared with me during our numerous discussions. His openness to dialog and constructive input have been indispensable for the successful outcome of this thesis.

Special thanks go to Daniel Britzger for his introduction to the Alpos software package, as well as numerous productive discussions on technical and theoretical topics. In addition, I would like to thank Markus Wobisch for his insight, as well as Giannis Flouris and Panos Kokkas for providing original code used by the CMS collaboration, which has been especially helpful for reproducing their results.

For the friendly and open atmosphere, I thank all of my colleagues at the IEKP.

Finally, I would like to thank my parents for their love and unwavering support throughout my studies.

Contents

1. Introduction

The field of high-energy physics is dedicated to the study of the fundamental components of matter and the interactions between them. The Standard Model of Particle Physics undoubtedly represents the broadest and most extensively tested theoretical model of these phenomena, having demonstrated a resounding success in describing the wealth of experimental data collected in high-energy collisions at particle accelerators.

Accordingly, a principal focus in high-energy physics has been the determination of Standard Model parameters from experimental data to a high degree of precision. In particular, precision studies of Quantum Chromodynamics (QCD), the theory of the strong interaction, have acquired greater importance in recent years, as an increasing number of phenomenological studies rely on precise QCD predictions. Aside from the masses of the quarks, the strong coupling constant α_s, conventionally evaluated at the scale of the Z-boson mass M_Z, is the only free parameter of QCD, and is currently among the least well known fundamental physical parameters.

Among the most promising experimental data from which the precision of $\alpha_s(M_Z)$ can be improved are measurements of jet production cross sections in hadron-induced collisions. Of these, measurements of inclusive jet production remain among the most precisely measured and well-understood observables.

The aim of this work is the development and implementation of a procedure for the determination of the strong coupling constant $\alpha_s(M_Z)$ from a combined dataset consisting of measurements performed in ep, pp and $p\bar{p}$ collisions at different scales.

The advantage of such a combined determination consists in the prospect of further improving the precision on $\alpha_s(M_Z)$ through the consideration of multiple datasets. In contrast to approaches involving a simple statistical combination of individually obtained estimates for $\alpha_s(M_Z)$, performing a determination on the basis of combined datasets ensures a consistent treatment of the measurements and theory calculations, as well as their uncertainties. In addition, this enables a detailed study of the compatibility of measurements and theory calculations, which may be obscured in a simple statistical combination.

In this work, such a procedure is developed and applied to datasets of inclusive jet cross section measurements performed by the H1, DØ, and CMS experiments. For each of these datasets, determinations of $\alpha_s(M_Z)$ have been performed by the respective experimental collaborations. This provides an important starting point for the development of a combined determination of $\alpha_s(M_Z)$, as well as serving as a direct comparison reference for its evaluation.

In the following chapters, the aspects relevant for these studies are presented. In chapter 2, the theoretical foundations relevant for high-energy hadron collisions, as well as

for the measurement and theoretical calculations of inclusive jet cross sections are outlined. The subsequent chapter 3 gives an overview of techniques for the estimation of theory parameters and their uncertainties. A review of the measurements and extractions of the strong coupling constant $\alpha_s(M_Z)$ performed by the individual experimental collaborations is provided in chapter 4.

Chapter 5 gives an overview of the software tools used for the implementation of the $\alpha_s(M_Z)$ determination, as well as outlining a number of aspects regarding numerical techniques. The development of the combined determination procedure and the results obtained for $\alpha_s(M_Z)$ are presented in chapter 6, along with a comparison to past $\alpha_s(M_Z)$ determinations. Finally, chapter 7 presents a summary of the main findings and explores ways for further extending and refining the $\alpha_s(M_Z)$ determination.

2. Theoretical Foundations

In the Standard Model of Particle Physics, the *strong interaction* is the fundamental interaction of color-charged elementary particles: *quarks* and *gluons*. It is distinguished from the other interactions by a number of unique characteristics which make it both interesting and challenging to study.

For instance, it is the only one of the four fundamental interactions for which the coupling strength α_s relates inversely to the energy scale of the interaction, giving rise to phenomena such as *color confinement* and *asymptotic freedom*. Both of these phenomena have far-reaching implications for the way strongly interacting systems manifest themselves in nature.

In this chapter, a brief overview of the Standard Model is given, with particular emphasis on the theory of the strong interaction. Furthermore, a number of aspects are discussed regarding the derivation of observable quantities and how these relate to the fundamental parameters of the theory.

2.1. The Standard Model of Particle Physics

The Standard Model of Particle Physics is a theory describing the properties and interactions of fundamental particles. Within this framework, each of the known fundamental particles is regarded as an excitation of a corresponding underlying quantum field, with interactions between them resulting from the principle of local gauge invariance.

There are four known fundamental interactions (also called *forces*) in nature: the electromagnetic interaction, the strong and weak nuclear interactions, and gravity. Of these, only the first three are described by the Standard Model.

The fundamental constituents of matter, the *fermions*, are particles with half-integer spin, while the particles responsible for mediating the fundamental interactions are called *bosons* and have integer spin. The Standard Model includes 12 types of fermions, which can be classified according to the interactions in which they participate. Of these, only the *quarks* carry color-charge, thus making them the only strongly interacting fermions. The remaining fermions are the *leptons*, which do not interact via the strong interaction. An overview of the fundamental particles described by the Standard Model can be seen in figure 2.1.

The dynamics of these fields can be described using the Lagrangian formalism. By postulating an appropriate *Lagrangian density* $\mathcal{L}$, the Euler-Lagrange equations of motion may be derived. In particular, this approach allows the conservation laws characterizing each of the fundamental interactions to be expressed as internal symmetries of the Lagrangian.

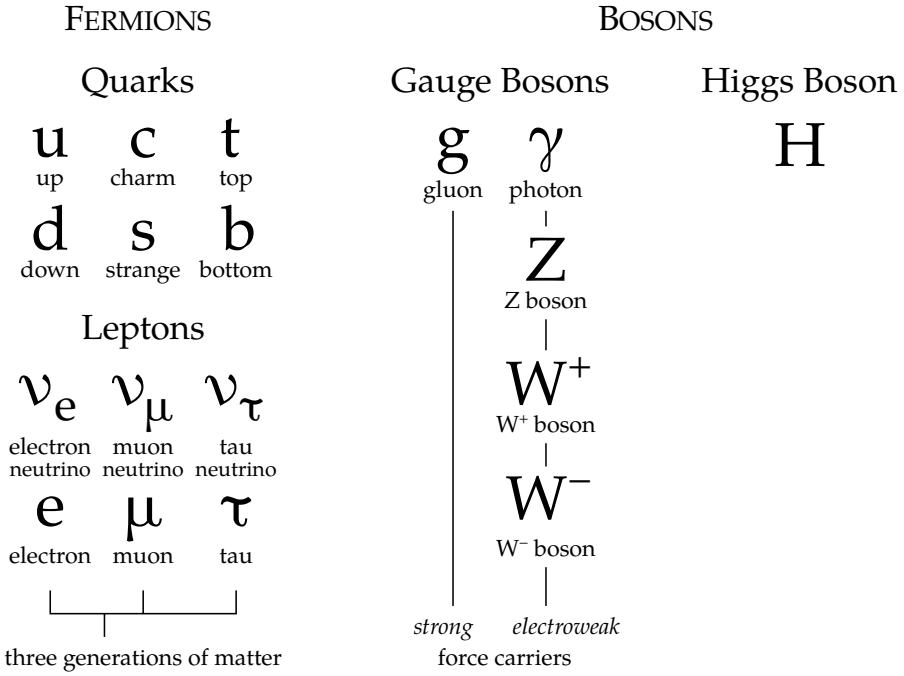

Figure 2.1.: Overview of the fundamental particles of the Standard Model. Fermions, half-integer spin particles that make up matter, are further divided into the color-charged quarks and the colorless leptons. Bosons have integer spin and include the gauge bosons, which mediate the fundamental interactions, and the Higgs boson. The gauge bosons of the strong interactions are called gluons. Due to electroweak symmetry breaking, the gauge bosons of the unbroken electromagnetic and weak interactions mix to form the carriers of the unified electroweak interaction.

Mathematically, the Standard Model Lagrangian exhibits a number of such symmetries. For instance, it is invariant under local gauge SU(3) transformations, codifying the conservation of color-charge in strong interactions. This is examined in more detail in section 2.2.

Another feature of the Standard Model Lagrangian is invariance under $\mathrm{SU(2)_L} \times \mathrm{U(1)_Y}$ transformations, which describe the unified electroweak interaction. Here, the subscript L refers to the fact that SU(2) transformations only act on left-handed spinors, while the subscript Y refers to *weak hypercharge*, the quantity conserved under the U(1) transformations.

However, the above $\mathrm{SU(2)_L} \times \mathrm{U(1)_Y}$ symmetry is only exact if the corresponding gauge fields are massless. Since three of the mediators of the electroweak interaction, the W and Z bosons, have mass, the symmetry is said to be spontaneously broken.

The Higgs mechanism allows for this symmetry to be recovered while also accommodating massive gauge bosons. By postulating an additional field ϕ with a non-zero energy ground state which also transforms covariantly under SU(2) × U(1) transformations, the resulting couplings of the W and Z bosons to this field give rise to non-zero mass terms in the Lagrangian. The photon, however, remains massless in the process, and the remaining degree of freedom of the Higgs field manifests itself as the physical Higgs boson. In a similar fashion, fermions also acquire mass by coupling to the Higgs field.

2.2. Quantum Chromodynamics

Quantum Chromodynamics (or QCD, for short) is the quantum field theory of the strong interaction. It formalizes the idea of color charge by introducing a Lagrangian which is invariant under local SU(N_c) gauge transformations, where $N_c = 3$ is the number of colors.

Mathematically, this makes QCD a non-abelian gauge theory, a property ultimately responsible for most of the particularities of QCD. The Lagrangian is given by:

$$\mathcal{L}_{\mathrm{QCD}} = \sum_q \bar{\psi}_{q,a} \left(\mathrm{i}\gamma^\mu \partial_\mu \delta_{ab} - g_\mathrm{s} \gamma^\mu t^C_{ab} \mathcal{A}^C_\mu - m_q \delta_{ab} \right) \psi_{q,b} - \frac{1}{4} F^{A\,\mu\nu} F^A_{\mu\nu} \tag{2.1}$$

Here, summation over repeated indices is implied. The quark fields for a particular quark flavor q have mass m_q and are denoted $\psi_{q,a}$, with the index a referring to the quark color and ranging from 1 to $N_c = 3$. The fields $\mathcal{A}^C_\mu$ represent the gauge (gluon) fields, with C ranging from 1 to ${N_c}^2 - 1 = 8$, and t^A are the eight generator matrices of the Lie algebra $\mathfrak{su}(3)$. The spinor algebra is handled by the Dirac matrices γ^μ, and δ_{ab} is the Kronecker delta.

The additional parameter g_s is a dimensionless quantity called the *coupling strength* of the interaction and is one of the free parameters of the theory, the other ones being the quark masses m_q. This quantity expresses the magnitude of the interaction between the different fundamental fields. In experimental high-energy physics, the term "coupling strength" conventionally refers to a different quantity, α_s, which is related to g_s by:

$$\alpha_\mathrm{s} = \frac{{g_\mathrm{s}}^2}{4\pi} \tag{2.2}$$

The field strength tensor $F^A_{\mu\nu}$ of the gluon field $\mathcal{A}^A$ is given in analogy to Quantum Electrodynamics by:

$$F^A_{\mu\nu} = \partial_\mu \mathcal{A}^A_\nu - \partial_\nu \mathcal{A}^A_\mu + g_\mathrm{s} f_{ABC} \mathcal{A}^B_\mu \mathcal{A}^C_\nu \tag{2.3}$$

However, since SU(3) is a non-abelian group, an extra contribution to the field strength tensor appears, which is proportional to the coupling g_s. The numbers f_{ABC}

are called the structure constants of $\mathfrak{su}(3)$, and are given by the commutation relations of the generators:

$$[t^A, t^B] = \mathrm{i} f_{ABC}\, t^C \tag{2.4}$$

Different terms in the Lagrangian correspond to different interactions between the fields. Each of the quark spinor fields ψ_q and $\bar{\psi}_q$ couple to the gluon field $\mathcal{A}$ with a coupling strength of g_s that is independent of the quark flavor. In addition, the third term in the field tensor (2.3), which arose as a consequence of the gauge group being non-abelian, leads to the self-coupling of the gluon field, giving rise to three and four-gluon interactions (see figure 2.2 in the next section).

It is this coupling of the gluons to each other that ultimately gives rise to a phenomenon called *confinement*, which implies that quarks cannot exist as free particles, but are confined to bound states called *hadrons*. This can be intuitively explained by the energy density of the gluon field between two quarks increasing as the quarks are separated, causing quark-antiquark pairs to be created from the vacuum, forming new hadrons.

Conversely, as the distance between two quarks tends toward zero, the strength of the interaction between them decreases as well. Thus, quarks behave as nearly free particles at low separation, a phenomenon called *asymptotic freedom*.

A more detailed explanation of how confinement and asymptotic freedom arise in the context of renormalization is addressed in section 2.2.2. The following section discusses how predictions for observable quantities are obtained in the framework of perturbative QCD.

2.2.1. Perturbative QCD

The equations of motion resulting from the QCD Lagrangian (2.1) are a system of inhomogeneous partial differential equations with no known analytic solution. Thus, the computation of theoretical predictions for observable quantities is typically done in perturbation theory.

In this approach, observable quantities are expressed as a power series in the coupling strength of the theory, α_s, which is assumed to be sufficiently small for the series to converge reasonably fast. Assuming F is an observable quantity, its perturbative expansion is given by:

$$F = \sum_{i=0}^{\infty} c_i\, {\alpha_\mathrm{s}}^i \tag{2.5}$$

Thus, calculating F is equivalent to determining the individual expansion coefficients c_i for each order in α_s. Although this would require computing an infinite number of coefficients in order to recover the exact quantity F, due to the original assumption of α_s being sufficiently small, truncating the perturbation series yields a reasonable approximation.

In particular, the scattering matrix elements relevant for predictions of scattering cross sections in particle collisions (see section 2.3) are obtained in this way. In this case, a finite number of contributions to the matrix elements may be derived from the Lagrangian for each order in α_s, and computed separately.

These individual contributions may be represented schematically as Feynman diagrams, which also encode the necessary information for constructing the associated mathematical expressions. Shown in figure 2.2, for instance, are the Feynman diagrams contributing to quark and gluon scattering in leading-order QCD.

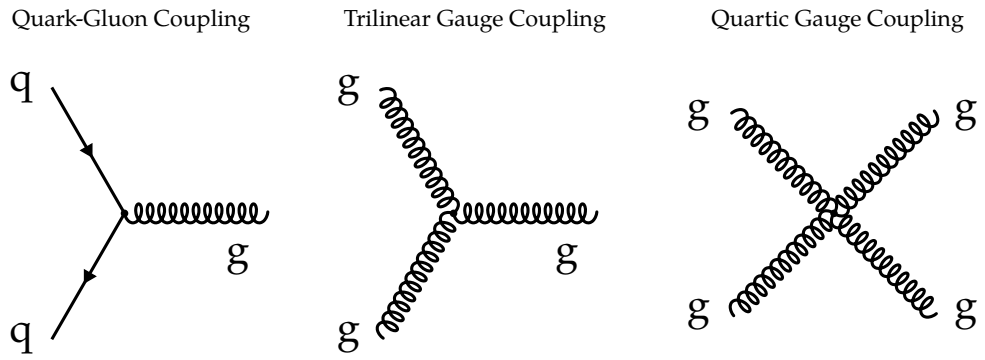

Figure 2.2.: Leading-order Feynman diagrams for QCD, showing the quark-gluon coupling and the two possible multi-gluon interactions.

In higher-order calculations, virtual particles also contribute to the matrix element. In contrast to initial and final state particles, the virtual particle kinematics are not uniquely determined, each requiring an additional integration over their phase space. Whenever these virtual particles occur in loops, the matrix element calculation may become divergent. The next section discusses how these divergences are treated.

2.2.2. The Running of the Strong Coupling

There are a finite number of Feynman diagrams contributing to a particular order in α_s. However, evaluating the integrals corresponding to particular higher-order terms involving loops may result in infinities. These are an artefact of the perturbative expansion and cancel out when the perturbation series is evaluated to all orders. Thus, in order to preserve the predictive power of fixed-order calculations, a meaningful way of subtracting these infinities is required. This is called *renormalization*.

In order to characterize the divergences occurring in loop integrals, a technique called *dimensional regularization* is used. This method introduces an additional dependence of the prediction on a parameter μ_R, which has the dimension of mass. This parameter is typically identified with the energy scale of the process being calculated.

Once this is done, renormalization can proceed by separating the divergent and finite parts of loop integrals in a systematic way. Thus, the offending infinities may be

subtracted from the divergent amplitudes, resulting in finite calculations to all orders. A side-effect of this procedure, however, is that the model parameters become dependent on the scale parameter μ_R. In particular, the coupling strength becomes scale-dependent, assuming different values for different energy scales of the interaction. This is called the *running of the strong coupling*:

$$\alpha_s = \alpha_s(\mu_R) \tag{2.6}$$

2.2.2.1. The Renormalization Group Equation

A natural consequence of (2.6) is that fixed-order predictions for observables also become dependent on the scale μ_R. Since this parameter is a direct consequence of the renormalization formalism, however, it must not affect the value of the full perturbation series (2.5), evaluated to all orders.

Formally allowing an observable F to depend on the renormalization scale μ_R in addition to its physical dependence on α_s, this condition can be expressed by requiring the total derivative of F with respect to μ_R to vanish:

$$\mu_R{}^2 \frac{\mathrm{d}}{\mathrm{d}\mu_R{}^2} F(\mu_R, \alpha_s) = \mu_R{}^2 \frac{\partial}{\partial \mu_R{}^2} F(\mu_R, \alpha_s) + \mu_R{}^2 \frac{\partial \alpha_s}{\mu_R{}^2} \frac{\partial}{\partial \alpha_s} F(\mu_R, \alpha_s) = 0 \tag{2.7}$$

The above expression is called the *renormalization group equation* (RGE), implying that the underlying structure of scale transformations is that of a group. In addition to enforcing the invariance of observable quantities under changes in scale, equation (2.7) also uniquely defines the necessary dependence of the coupling strength on the renormalization scale:

$$\mu_R{}^2 \frac{\partial \alpha_s}{\partial \mu_R{}^2} = \beta(\alpha_s) \tag{2.8}$$

In the above relation, $\beta(\alpha_s)$ does not depend explicitly on the renormalization scale, and can be calculated by solving the RGE in (2.7). Typically, it is also expressed as a perturbation series in α_s:

$$\beta(\alpha_s) = -(b_0 \alpha_s{}^2 + b_1 \alpha_s{}^3 + b_2 \alpha_s{}^4 + \ldots) \tag{2.9}$$

Performing the calculation of $\beta(\alpha_s)$ reveals an overall negative sign, which has been explicitly indicated in (2.9). Thus, the renormalized coupling $\alpha_s(\mu_R)$ decreases as the energy scale of the interaction increases, implying that, in the high-energy limit, QCD behaves increasingly like a free theory. This is known as *asymptotic freedom*.

At low energies, the converse is true, and the QCD coupling becomes increasingly large. One consequence of this is that, as the value of α_s surpasses unity, the perturbation series postulated in (2.5) diverges. Perturbative QCD calculations thus lose their predictive power for low-energy systems, which require phenomenological models for their description.

Physically, the significance of a large coupling is that quarks can never be found in isolation. Were this the case, the energy density of the gauge field would increase sufficiently to polarize the vacuum and create new quarks, forming bound hadrons. This phenomenon is called *confinement*.

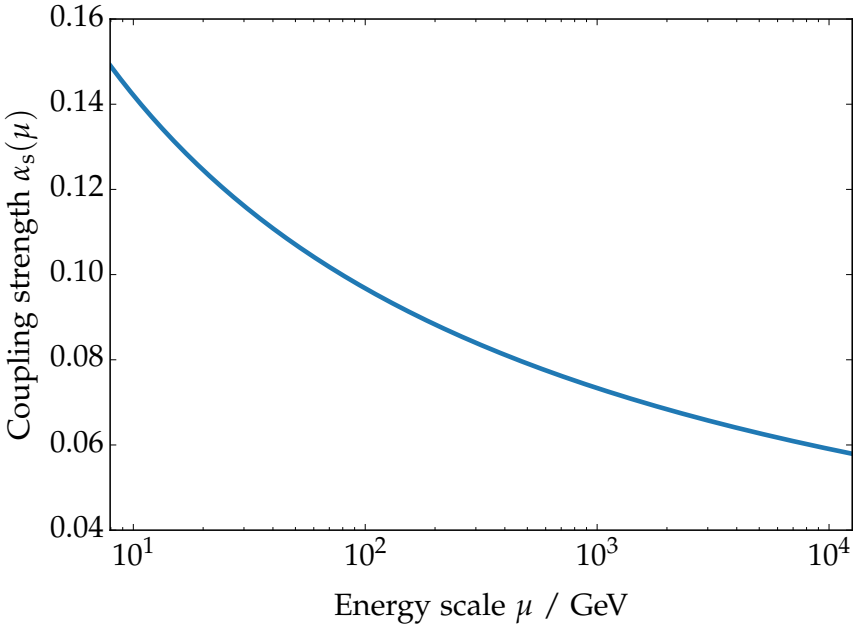

Figure 2.3.: Sketch of the running of α_s.

Since α_s is a free parameter of QCD, its value, which is conventionally given at the energy scale of the Z-boson mass M_Z, must be determined by comparing theory predictions of observables to experimental measurements. The next section outlines scattering experiments typically performed in high-energy physics.

2.3. QCD in Hadronic Particle Collisions

Most experiments in particle physics are scattering experiments conducted at particle colliders. By accelerating projectile particles to high center-of-mass energies and colliding them together, they undergo an inelastic scattering process to produce a number of final-state particles, the properties of which can then be measured in a detector.

The aim of these experiments is determining the empirical probability of the scattering resulting in a specific final state. To this end, such measurements are repeated a large number of times.

The probability of producing a certain configuration of particles in the final state is dependent on the quantum field theoretic amplitude of that process and the kinematics of the final state, as well as on experimental variables, such as the size, particle den-

sity and overlap of the particle beams. In order for measured reaction rates to remain comparable across experiments, they are normalized to the particle flux, also called the *luminosity* L. This results in a measure of the interaction probability which is independent of experimental parameters, the cross section σ:

$$\sigma = \frac{\mathrm{d}N}{\mathrm{d}t} \frac{1}{L} \tag{2.10}$$

The name "cross section" is chosen in analogy to the related concept in classical scattering theory, where the interaction rate is proportional to the cross sectional area of the scattering bodies. It is conventionally measured in *barn* (b), a unit of area corresponding to $10^{-28}\,\mathrm{m}^2$.

Cross sections may be of different types, depending on the requirements placed on the final state being considered. They are said to be *inclusive* if events with additional collision products with respect to the considered final state are also included in the measurement. Otherwise, cross sections are said to be *exclusive*.

In addition, cross sections may also be measured differentially with respect to quantities characterizing the final state. For instance, differential cross sections are often measured as a function of kinematic variables, such as transverse momentum p_T, or purely geometric ones, such as the detection angle.

Due to a large number of elementary scattering processes involving quarks and gluons, QCD plays an important part in performing the calculation of cross section predictions for these processes. However, working in the framework of perturbative QCD requires the coupling strength to be significantly less than unity. This translates to a restriction on the energy scale of the interactions for which cross sections can be calculated. More precisely, perturbative QCD can only be used to compute high-energy scattering.

There are, however, a number of phenomena characterized by energy scales at which QCD becomes non-perturbative. In this case, a phenomenological approach must be taken. One such intrinsically non-perturbative phenomenon is the hadronization of color-charged particles in the final state, which is addressed in section 2.3.2. Another concerns the initial state of the scattering, which may consist partly or entirely of hadrons. This requires a description of the hadron composition, which is outlined in section 2.3.1.

2.3.1. The Parton Model of Hadrons

Deep inelastic scattering experiments have revealed that protons are not fundamental, point-like particles. Instead, they are made up of quarks and gluons, collectively called *partons*. In the parton model, hadrons such as the proton are held together by the strong interaction between the partons. These interactions are termed *soft*, since their characteristic energy scale is comparatively low. Indeed, perturbative approaches fail in describing hadron structure, since the assumption of a small coupling strength α_s no longer holds for these energies.

Thus, no complete model of high-energy proton scattering is available in perturbative QCD. Nevertheless, it is possible to describe these processes using mixed models

combining perturbative techniques with phenomenological models of the proton composition.

To this end, the calculation of these processes is factorized into two parts. The parton scattering itself occurs at a sufficiently high energy to be calculated in perturbative QCD, and is therefore termed *hard*. Conversely, the intrinsically soft proton structure is described phenomenologically by postulating probability distributions for the parton kinematics. In this section, this calculation technique is reviewed in the context of deep inelastic electron-proton scattering.

2.3.1.1. Deep Inelastic Scattering

Historically, the first evidence of proton substructure came from a particular class of experiments called *deep inelastic scattering* (DIS). By measuring the energy dependence of the electron-proton scattering cross section, experimental data was shown to deviate from predictions assuming point-like protons. Furthermore, protons were seen to disintegrate at sufficiently high energies, forming hadronic final states. These observations revealed protons to be bound states of strongly interacting particles.

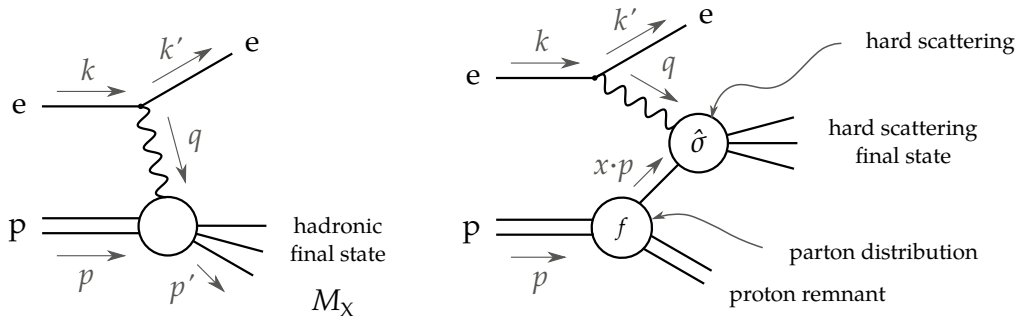

Figure 2.4.: *(left)* Kinematics of deep inelastic scattering. An electron and a proton with four-momenta k and p, respectively, interact by exchanging a particle with four-momentum q. While the electron is simply scattered, the proton disintegrates into a number of mainly hadronic particles, with a total invariant mass M_X. *(right)* Factorization of deep inelastic scattering. The electron scatters off a parton carrying a fraction x of the total proton momentum.

Electron-proton DIS processes (shown in figure 2.4, *left*) are characterized by three quantities: the total energy $\sqrt{s}$ of the system in the center-of-mass frame, the magnitude $Q^2 = -q^2$ of the four-momentum transferred between the two particles, and the dimensionless Bjorken scaling variable x, defined as:

$$x = \frac{Q^2}{2p \cdot q} \tag{2.11}$$

As can be seen from (2.11), this variable is manifestly Lorentz-invariant. It represents,

in a sense, the degree to which the scattering is inelastic. At $x = 1$, the proton remains intact, scattering elastically off the electron. At $x \ll 1$, the proton disintegrates into a final state with an invariant mass $M_X \gg M_p$. This is deep inelastic scattering.

In the partonic view, the scattering occurs between the highly energetic electron and one of the proton's component partons (figure 2.4, *right*). At sufficiently high energies, the Bjorken scaling variable x is a good approximation of the fraction of the total proton momentum carried by the participating parton.

Thus, the description of DIS processes can be seen as consisting of two parts, each with a different characteristic energy scale: the hard scattering, which can be calculated in perturbative QCD, and the soft proton structure, which must be described phenomenologically.

To this end, an additional, arbitrary energy scale μ_F is introduced, called the *factorization scale*. This quantity represents the energy threshold separating the soft and hard energy regimes, allowing such processes to be factorized into two parts in a well-defined manner. This technique necessarily introduces a dependence of the hard cross section $\hat{\sigma}$ on the factorization scale μ_F, in addition to the renormalization scale dependence resulting from perturbative QCD.

2.3.1.2. Parton Distribution Functions

The parton model aims to provide a phenomenological description of the kinematics of hadron constituents. This is done by introducing probability distributions over x, the fraction of proton momentum carried by the parton.

At an energy scale μ_F, the probability density of finding a parton with flavor j carrying a fraction x of the proton momentum is denoted $f_j(x, {\mu_F}^2)$ and is called a *parton distribution function*, or PDF, for short. This allows the DIS cross section to be written as a convolution of the hard cross section $\hat{\sigma}$ and the PDF:

$$\sigma_{DIS} = \sum_j \int \mathrm{d}x \; f_j(x, {\mu_F}^2) \times \hat{\sigma}_j(xs, {\mu_R}^2, {\mu_F}^2) \tag{2.12}$$

The μ_F dependence of observable quantities, as suggested by (2.12), must vanish in the perturbative limit (2.5). Since a change in μ_F merely represents a redistribution of contributions from the PDFs to the hard cross section, this requirement imposes a restriction of the way PDFs transform under a change of scale.

In leading-order QCD, this may be expressed as follows:

$${\mu_F}^2 \frac{\partial f_i(x, {\mu_F}^2)}{\partial {\mu_F}^2} = \sum_j \frac{\alpha_s({\mu_F}^2)}{2\pi} \int_x^1 \frac{\mathrm{d}\xi}{\xi} P_{ij}^{(1)}(\xi) f_i\left(\frac{x}{\xi}, {\mu_F}^2\right) \tag{2.13}$$

These are known as the leading-order QCD evolution equations, also called the DGLAP evolution equations, named for the authors by whom they were first derived [1–3]. Here, $P_{ij}^{(1)}(\xi)$ is the leading-order splitting function, which expresses the likelihood

of a parton of flavor j carrying a fraction ξ of the proton momentum emitting a parton of flavor i.

Thus, QCD provides the appropriate tools to describe the μ_F dependence of PDFs. However, the probability distribution of x itself is not predicted by the theory. Rather, it must be determined by performing fits to experimental data. In this respect, DIS scattering provides a direct handle on the PDFs through (2.12), although pure hadron scattering cross sections (see section 2.3.1.3) may also be used for further constraining these.

There are a number of different approaches to PDF determination, with a number of groups specializing in determining so-called *global* PDF sets using data from multiple measurements. [4–11] The obtained PDF sets are different in terms of the PDF parametrization, the measurements entering the fit, the method of calculating theory predictions, as well as other procedural details.

2.3.1.3. Generalization to Pure Hadronic Scattering

In DIS, the initial-state lepton reduces the expression for the cross section to a single convolution between the PDF and the hard scattering. In hadron-hadron collisions, the structure of both initial-state hadrons must be accounted for in the cross section, leading to a double convolution.

Specifically, the cross section for the production of a final state X in proton-proton collisions is given by: [12]

$$\sigma(\mathrm{pp} \to \mathrm{X}) = \sum_{ij} \int \mathrm{d}x_1 \, \mathrm{d}x_2 \; f_i(x_1, {\mu_F}^2) f_j(x_2, {\mu_F}^2) \times \hat{\sigma}_{ij \to \mathrm{X}}(x_2 x_1 s, {\mu_R}^2, {\mu_F}^2) \tag{2.14}$$

Here, the hard process is the scattering of a parton of flavor i from one of the incoming protons off a parton of flavor j from the other.

2.3.2. Jets

Color confinement dictates that free particles cannot have a net color charge. Consequently, quarks and gluons in the final state of a hard scattering process undergo hadronization and are detected as collimated streams of particles, called *jets*. Moreover, due to the relatively high coupling strength of QCD with respect to the other interactions, most hadron-induced processes result in jets.

Jet-related observables therefore provide a valuable experimental handle on QCD. In particular, inclusive jet cross sections constitute a well-defined observable, both from an experimental and a theoretical point of view. This makes them ideally suited for estimating the free parameters of QCD by comparing measurement data to theory predictions.

Nevertheless, measurements and predictions of jet-related observables introduce new challenges due to the high particle multiplicity typical of jet events, requiring robust jet

reconstruction techniques. An essential part of this is the methods used for clustering the final-state particles to jets, for which several methods exist. These are presented in the following.

2.3.2.1. Jet Clustering Algorithms

Due to quark and gluon fragmentation and subsequent hadronization, the resulting jets consist of a high number of particles, most of which are measured within the same region of the detector. Thus, an important task for measuring jet-related observables is establishing a method of clustering these particles in order identify the jets and reconstruct the final-state quark or gluon from which they originated. For this, a number of algorithms exist, of which two broad categories are reviewed here.

Cone-based clustering algorithms focus on identifying the so-called stable cones in the final-state geometry, which are each taken to correspond to one reconstructed jet. This is typically done by iteratively restructuring an initial cone configuration based on the kinematics of the particles detected within it until a stable configuration is reached. The specifics of this process depend on the particular algorithm.

In contrast to cone-based algorithms, *sequential clustering* algorithms make no assumption regarding the shape of the jets. Instead, these involve the definition of a distance measure between reconstructed final-state particle four-momenta, based on geometric and kinematic variables. The algorithm then proceeds to combine pairs of four-momenta with minimal separation according to the defined metric, repeating the process until all remaining four-momenta meet a specific stopping criterion. The resulting particle clusters are identified as jets.

Prominent examples of sequential clustering algorithms are the k_T [13], and anti-k_T [14] algorithms. These are also used for jet reconstruction in the H1 and CMS inclusive jet measurements discussed in chapter 4. Also discussed is the DØ inclusive jet measurement, where jet reconstruction is done using a cone-based algorithm, which is described in [15].

2.3.3. Non-Perturbative Effects

Perturbation theory is a powerful tool for calculating hard scattering processes in QCD. There are, however, additional processes occurring in hadron-induced scattering processes which prove impossible or challenging to handle perturbatively.

In jet measurements, one such process is that of parton fragmentation and hadronization, which connects the partonic final state of the hard scattering with the particles observed in the detector. Furthermore, additional contributions to the cross section may appear as a result of interactions outside the hard scattering process, such as additional hard and soft QCD interactions or multiple parton interactions.

A common approach to including these effects in data-theory comparisons and parameter estimations is the introduction of a number of multiplicative correction factors, which are determined using Monte Carlo simulations and are applied to the fixed-order theory predictions. Since the obtained factors highly depend on the specific method of

derivation, an additional systematic uncertainty source is also typically introduced to reflect this.

3. Parameter Estimation

While physical theories provide predictions for observable quantities, these typically depend on a number of *free parameters*, for which the theories themselves make no prediction. Rather, they must be inferred (or *fitted*) by comparing the theoretical predictions for an observable quantity to experimental measurements.

Due to the intrinsic randomness of the measurement process, however, the inference of theoretical parameters from data can only be performed using stochastic methods. As a consequence, the estimates obtained for parameters in this way are subject to an uncertainty, which must be quantified.

In this chapter, the *maximum likelihood* and *least squares* approaches to parameter estimation and a number of its generalizations are discussed, and a number of categories of experimental and theoretical uncertainties are identified. Finally, a number of methods for obtaining estimates for parameters and their uncertainties are presented.

3.1. Experimental and Theoretical Uncertainties

The observable quantities central to high-energy physics are the scattering cross sections for a wide array of elementary processes. These are experimentally determined at particle collider experiments by accelerating subatomic particles and colliding them at high energies. The products of these collisions are measured in particle detectors.

Such measurements, however, are subject to a large number of effects which limit their accuracy and precision. A large part of the experimental analysis, therefore, consists in identifying these effects and estimating the magnitude of the associated uncertainties on the measurements. Furthermore, uncertainties also arise in theoretical calculations of cross sections. In this section, several types of uncertainties arising within these contexts are presented and a number of stochastic methods allowing for their formal treatment are introduced.

3.1.1. Statistical and Systematic Uncertainties

One type of uncertainty arises due to statistical fluctuations in measured quantities. Since only a finite sample of measurements is used for determining cross sections experimentally, the resulting estimates acquire a statistical uncertainty, which decreases with the number of measurements per sample. Since these estimates are derived from event counts per time interval, the corresponding fluctuations are commonly modeled using a Poisson probability distribution. For sufficiently small effects, a Gaussian distribution can be substituted.

Furthermore, owing to the complexity of the measuring apparatus, a multitude of systematic factors also affect the measurement. While the experimental setup can be finely calibrated to reduces the size of these effects, they cannot be completely eliminated, resulting in a systematic uncertainty on the measurement.

The origin and magnitude of systematic effects is highly dependent on the experimental setup and the particular measurement methodology. For instance, uncertainties on cross section measurements at hadron colliders can be traced back to the uncertainties in the determination of experimental parameters such as instantaneous luminosity, trigger efficiencies, or the energy calibration and intercalibration of the different detector components. For jet-related measurements in particular, this is supplemented by systematic effects relating to jet resolution and jet energy calibration, as well as uncertainties arising due to unfolding strategies.

Likewise, theory predictions for cross sections are also subject to the two types of uncertainties outlined above. Statistical fluctuations of theory calculations arise due to intrinsically random calculation techniques, such as Monte Carlo integration or the modeling of particle decays as Markov processes, both being extensively used in high-energy physics.

As with experimental measurements, theory predictions are also subject to systematic uncertainties. A prominent example are so-called "scale" uncertainties arising in the context of fixed-order perturbative calculations. Due to the truncation of the perturbation series, the predictive power of fixed-order theory predictions is limited. In the context of renormalization (see section 2.2.2), given the invariance of the complete perturbative series for observables under a change in the renormalization scale μ_R, an estimate for the magnitude of this effect is obtained by evaluating the dependence of fixed-order predictions on μ_R. Similarly, the scale dependence arising from factorizing hadronic scattering cross sections into the perturbative hard process and the soft hadron composition expressed as PDFs (see section 2.3.1) gives rise to a similar systematic uncertainty.

Naturally, the effects described above place limits on the ability of extracting precise and accurate estimates of theory parameters from the measured data. These must be taken into account by the estimation procedure. This is typically achieved by postulating a probabilistic model for the measurements, using statistical inference methods, as described in the next section.

3.1.2. Stochastic Modeling of Uncertainties

An essential prerequisite for any parameter estimation procedure consists in establishing a means of quantifying the uncertainties. For this purpose, observed and calculated quantities are modeled stochastically as realizations of random variables drawn from probability distributions. This allows both the quantities and the uncertainties to be expressed in terms of the parameters of these distributions. In the following, the standard assumption of a Gaussian distribution for modeling these effects is presented, and a number of implications for the resulting error model are discussed.

A standard approach to modeling the uncertainty of measured or calculated quanti-

ties is based on the assumption of a Gaussian distribution, identifying the unobserved "true" value of the quantity with the location parameter μ, and the uncertainty with the scale parameter σ. This can be expressed as:

$$X \sim \mathcal{N}(\mu = x_0, \sigma) \tag{3.1}$$

Here, X denotes the random variable representing the uncertain quantity, $\mathcal{N}$ refers to the Gaussian distribution, and x_0 denotes the true value. In this model, the expectation value $\langle X \rangle$ and the variance $\mathrm{Var}(X)$ of the uncertain quantity coincide with the true value and the square of the uncertainty, respectively. In the context of a finite statistical sample of measurements, the parameters μ and σ of the above Gaussian distribution can be estimated, respectively, as the mean and standard deviation of the sample. Consequently, these parameters acquire a well-defined statistical interpretation.

Owing to the central limit theorem, this model is adequate for uncertainties resulting from the contribution of several independent random effects. However, not all experimental effects can be described in this way. For instance, statistical fluctuations in counting experiments are best modeled by means of a Poisson distribution. For sufficiently small effects, however, a Gaussian distribution remains a good approximation, and can be substituted readily.

The above assumption is equivalent to modeling the random value X as the sum of the true value x_0 and a random additive contribution drawn from a Gaussian distribution with $\mu = 0$:

$$X \sim x_0 + \mathcal{N}(\mu = 0, \sigma) \tag{3.2}$$

This is of particular relevance when discussing uncertainties arising from random *multiplicative* contributions. In this case, the expression obtained for the random quantity X results from applying the Gaussian hypothesis to a multiplicative factor. In order to recover the true value x_0 as the expectation $\langle X \rangle$, the random factor is drawn from a Gaussian distribution with $\mu = 1$. The scale parameter σ corresponds to the uncertainty of the factor, σ^*, and thus to the relative uncertainty of the quantity X:

$$X \sim x_0 \cdot \mathcal{N}(\mu = 1, \sigma = \sigma^*) \tag{3.3}$$

In both the additive (3.2) and multiplicative (3.3) models, the distribution of the additive and multiplicative factors is considered to be determined entirely by the experimental circumstances, and thus the parameters μ, σ and σ^* are generally not permitted to depend on the true value x_0.

It is worth noting that a prerequisite of some methods of parameter estimation consists in the assumption of an additive Gaussian uncertainty model. This is, for instance, the case with least squares estimation, which is described in the following section. Consequently, multiplicative effects must be treated as additive.

One possibility of achieving this is to allow the scale parameter σ to change as a function of the estimated true value, and thus as a function of the theory parameters. Alternatively, the multiplicative relation in (3.3) may be turned into an additive one by ap-

plying the logarithm. In order to recover the Gaussian distribution in the transformed quantity, the Gaussian distribution in (3.3) is replaced by a log-normal distribution:

$$X \sim x_0 \cdot \ln \mathcal{N}(\mu = 1, \sigma = \sigma^*) \tag{3.4}$$

Due to the similarity of the Gaussian and log-normal distributions for small values of σ^*, this substitution is justified in cases for which the relative uncertainty is sufficiently small.

Applying the logarithm then reduces the multiplicative measurement model to an additive model involving the logarithm of the measured quantity:

$$\ln X \sim \ln x_0 + \mathcal{N}(\ln \mu = 0, \sigma^*) \tag{3.5}$$

Here, the second term on the right hand side refers to a normally distributed random variable with scale parameter σ^*, and results from applying the logarithm to the log-normal distribution assumed for multiplicative uncertainties. The variance of this expression is $\mathrm{Var}(\ln X) = \sigma^*$.

The stochastic models presented above, allow well-known statistical procedures for parameter estimation to be applied. In the following, the *maximum likelihood* and related *least squares* approaches to parameter estimation are presented.

3.2. Maximum Likelihood and Least Squares Estimation

The primary goal of parameter estimation lies in determining the theory parameter values for which the theory predictions best fit the measurement data. In practice, this amounts to defining a quantity expressing the level of agreement between the data and the theory predictions. Finding the best estimate for the theory parameters is then equivalent to finding the parameter values for which this quantity attains its global extremum, indicating a maximal level of agreement between the theory and the data.

Multiple ways of expressing the agreement between the data and the theory predictions exist. One approach to establishing a unique definition consists of constructing an expression for the probability of observing a particular outcome in measurements, as a function of the theory parameters called the *likelihood function*. Accordingly, this approach is called *maximum likelihood* parameter estimation.

In the following, as a starting point, an array $\mathbf{m}$ of N measurements m_i is considered. The corresponding theory predictions t_i are functions of the theory parameters $\mathbf{a}$.

A prerequisite for the maximum likelihood method is postulating a probability distribution for the individual measurements. A standard choice, motivated by the central limit theorem is that of a Gaussian distribution. By identifying the location parameter μ of the Gaussian distribution with the theory prediction and the scale parameter σ with the experimental uncertainty, the individual likelihood of each measurement can

be expressed as:

$$L_i(\mathbf{a}) = L(m_i \mid t_i(\mathbf{a}), \sigma_i) = \frac{1}{\sqrt{2\pi}\sigma_i} \exp\left(-\frac{(m_i - t_i(\mathbf{a}))^2}{2{\sigma_i}^2} \right) \tag{3.6}$$

When considering independent measurements, the likelihood of observing all measurements simultaneously is the product of the likelihoods of observing the measurements individually:

$$L(\mathbf{a}) = \prod_i L_i(\mathbf{a}) \tag{3.7}$$

Best estimates for the theory parameters $\mathbf{a}$ are then obtained by finding the global maximum of the above expression. In general, this is a multidimensional optimization problem, and is handled using numerical techniques.

In the case of the Gaussian uncertainty model illustrated above, it is possible to define an equivalent formulation of the maximum likelihood estimation procedure by deriving an alternative expression to the likelihood function (3.7), which remains maximal when evaluated at the best estimate for $\mathbf{a}$.

One such alternative expression may be derived upon the realization that the exponential map appearing in (3.6) is a monotonous function. Therefore, its extrema always coincide with the extrema of its argument, meaning that it is sufficient to maximize the logarithm of the likelihood function (3.7), or, more conventionally, to minimize the negative logarithm, multiplied by a factor of two for convenience. The quantity obtained is:

$$-2 \ln L\,(\mathbf{a}) = \sum_i \left(\frac{m_i - t_i(\mathbf{a})}{\sigma_i} \right)^2 + \text{const.} \tag{3.8}$$

Here, the product of exponentials in (3.7) becomes a sum of their respective arguments, and the constant normalization factors in (3.6) become additive constants, which have no bearing on the minimization, and can thus be set to zero. The expression above is then reduced to a sum of the squares of the differences between the measurements and the theory predictions, normalized to the experimental uncertainty. This quantity is called the *least squares estimator* and is commonly denoted χ^2:

$$\chi^2 = \sum_i \left(\frac{m_i - t_i(\mathbf{a})}{\sigma_i} \right)^2 \tag{3.9}$$

This notation is an indication that, being the sum of squares of normally distributed quantities, the probability distribution of this quantity is the χ^2 distribution. This probability distribution is characterized by a single parameter, the *number of degrees of freedom*, denoted "ndf".

Assuming the Gaussian uncertainty model is correct, the least-squares estimator fol-

lows a χ^2 distribution with ndf $= N_{\text{dat}} - N_{\text{par}}$, where N_{par} is the number of free parameters and N_{dat} is the number of measurements. The value of the χ^2 quantity in the minimum therefore enables an evaluation of the fit quality. This is conventionally expressed in terms of the *reduced* χ^2 quantity, χ^2/ndf, which is expected to be approximately equal to unity.

3.2.1. Generalizations and Refinements

Equation (3.9) can also be written in compact form by defining a *residual vector* $\mathbf{p} = \mathbf{m} - \mathbf{t}(\mathbf{a})$ and a *variance matrix* $\mathbf{V}$, a diagonal matrix containing the variances of the measurements, which are equal to the squares of the uncertainties σ_i:

$$\chi^2 = \mathbf{p}^\top \mathbf{V}^{-1} \mathbf{p} \tag{3.10}$$

Since this quantity only involves simple linear algebra operations, it is more straightforward and efficient to compute than the full likelihood function. As a result, least-squares estimation has found extensive use for determinations of physical parameters.

The main limitation of this procedure lies in the requirement that the measurements be drawn from a Gaussian distribution. Owing to the central limit theorem, this is generally understood to be a satisfactory assumption for experimental uncertainties generated by a large number of random additive effects on the measurements.

The correct treatment of uncertainties arising from multiplicative effects, however, requires additional considerations. Furthermore, since a number of random effects may affect a set of measurements in a correlated way, this must also be accounted for when defining a χ^2 quantity.

One generalization of least squares estimation can be made for correlated uncertainties. For any sequence $\tilde{\mathbf{x}}$ of correlated random variables, a linear transformation $\mathbf{B}$ can be found, such that the transformed variables $\mathbf{x} = \mathbf{B}\tilde{\mathbf{x}}$ are independent. Applying this reasoning to the residual vectors $\tilde{\mathbf{p}}$ for correlated measurements, leads to additional matrix-valued factors in (3.10), which can be absorbed by the variance matrix:

$$\chi^2 = \mathbf{p}^\top \mathbf{V}^{-1} \mathbf{p} = \tilde{\mathbf{p}}^\top \mathbf{B}^\top \mathbf{V}^{-1} \mathbf{B}\, \tilde{\mathbf{p}} = \tilde{\mathbf{p}}^\top \tilde{\mathbf{V}}^{-1} \tilde{\mathbf{p}} \tag{3.11}$$

In the above expression, the matrix $\tilde{\mathbf{V}}$ is the *variance-covariance matrix* of the measurements, or simply the *covariance matrix*. Thus, correlated measurements can be handled in least squares estimation by including the covariances of the measurements in (3.10). Throughout this work, the tildes used above to refer to correlated quantities are omitted, since this information is contained in the covariance matrix itself.

A further aspect concerns the incorporation of multiple uncertainty sources into the uncertainty model, in particular the inclusion of uncertainties on the theory in the χ^2 definition. In this case, the total uncertainty on the residual vector $\mathbf{p} = \mathbf{m} - \mathbf{t}(\mathbf{a})$ results from the cumulated uncertainties on the measurement and the theory predictions. If these uncertainties are assumed to be Gaussian in nature, the linearity of variances allows this to be handled by adding together the covariance matrices corresponding to

the different uncertainty sources, thus constructing a total covariance matrix.

The above formulation models the uncertainty as arising from random additive contributions drawn from a constant, Gaussian probability distribution. However, when considering multiplicative effects, which are inherently proportional to the quantity whose uncertainty they describe, the distribution becomes non-Gaussian, and several of the assumptions made above no longer hold exactly.

Rather, multiplicative effects on observables are best modeled in terms of the uncertainty relative to the true value of the observable, which is assumed to be constant. One possibility of handling these uncertainties is to allow the covariance matrix in (3.10) to become a function of the minimization parameters.

An alternative approach involves modeling the effect of a multiplicative uncertainty on measurements and theory predictions by means of a log-normal probability distribution, with the scale parameter σ^* corresponding to the relative uncertainty of the observed or calculated quantity. This is equivalent to postulating a Gaussian distribution for the logarithms of the original quantities (see section 3.1.2), thus allowing least squares parameter estimation to be performed in the logarithmic domain. The χ^2 quantity is redefined accordingly as:

$$\chi^2 = \sum_{ij} \left(\log \frac{m_i}{t_i(\mathbf{a})} \right) \left[\mathbf{V}_{\text{rel}}{}^{-1} \right]_{ij} \left(\log \frac{m_j}{t_j(\mathbf{a})} \right) \tag{3.12}$$

Here, the covariance matrix is computed using relative uncertainties, reflecting the scale parameter σ^* of the log-normal distribution.

If the magnitude of uncertainties on a particular quantity are small with respect to the value of the quantity, both the Gaussian and the log-normal approach yield comparable estimates.

3.2.2. Fully Correlated Uncertainties

In the above sections, the treatment of correlations between measurements is approached by the introduction of covariance matrices, which can be determined independently for each contribution to the uncertainty and added together to form the total covariance matrix appearing in the χ^2 quantity. For fully correlated contributions to the uncertainty, the correlation coefficient between any two measurements is exactly equal to unity. Mathematically, this is equivalent to assuming that the random fluctuation associated with the uncertainty affects all measurements in equal measure.

An alternative to including this uncertainty in the covariance matrix consists in the introduction of an additional so-called *nuisance parameter* ε representing the value of the random fluctuation affecting all measurements.

In this case, the χ^2 can be expressed as:

$$\chi^2 = \sum_{ij} \left(m_i - t_i(\mathbf{a}) + \varepsilon \cdot \sigma_i \right) \left(\mathbf{V}^{-1} \right)_{ij} \left(m_j - t_j(\mathbf{a}) + \varepsilon \cdot \sigma_j \right) + \varepsilon^2 \tag{3.13}$$

Here, the σ_i are the uncertainties of each point associated with the fully correlated fluctuation. The final term is a reflection of the constraint placed on the parameter ε, requiring it to be drawn from a standard normal distribution.

Compared to the traditional approach using covariance matrices, the nuisance parameter approach has the advantage of allowing the magnitude of fully correlated effects to be ascertained. The values obtained for the nuisance parameters after minimization are expected to be distributed around zero with a variance of unity. A large deviation of a particular nuisance parameter from zero may be considered symptomatic of a poor fit quality.

3.3. Estimation of Uncertainties

The minimization of the χ^2 quantity with respect to the theory parameters $\mathbf{a}$ yields a best estimate for the parameters, denoted here as $\hat{\mathbf{a}}$. Due to the inherent uncertainty of the measurements and theory predictions, expressed as a covariance matrix $\mathbf{V}$, the estimated parameters are also subject to an uncertainty. Taking into account parameter correlations, this uncertainty can be expressed as a covariance matrix, which is denoted $\mathbf{V}_\mathrm{a}$. The vector $\hat{\sigma}_\mathrm{a}$, composed of the square roots of the diagonal entries of $\mathbf{V}_\mathrm{a}$, is defined as the uncertainty vector of the parameters.

Linear Error Propagation

A straightforward way of obtaining the matrix $\mathbf{V}_\mathrm{a}$ exists for problems for which the theoretical model $\mathbf{t}(\mathbf{a})$ is a linear function of its parameters. For this, it can be shown that the vector of parameter estimates $\hat{\mathbf{a}}$ can be computed analytically as a linear function of the measurements $\mathbf{m}$. Thus, the covariance matrix $\mathbf{V}$ can be propagated through this expression in order to obtain the parameter covariance matrix $\mathbf{V}_\mathrm{a}$. This is termed *linear error propagation*.

In practice, even linear problems are solved by minimizing the χ^2 quantity using numeric methods. Thus, the parameter covariance $\mathbf{V}_\mathrm{a}$ is not calculated analytically, but must be estimated numerically. A helpful consideration in this case is the fact that, for linear problems, the χ^2 function (3.10) is a quadratic form over both the measurement space and the parameter space.

Since taking the (matrix-valued) second derivative of the χ^2 quantity with respect to the measurements $\mathbf{m}$ yields a quantity equal to twice the inverse covariance matrix $\mathbf{V}^{-1}$, the parameter covariance matrix is defined accordingly as half the inverse of the second derivative of the χ^2 quantity with respect to the parameters. This is equivalent to the analytic *linear error propagation* described above, but can be calculated numerically. This is also called the *Hessian* method, in reference to the name given to the second derivative matrix.

χ^2 Profiling

For nonlinear problems, the error estimates obtained through the methods described above are no longer reliable. Since for nonlinear models, the Gaussian assumption no longer holds for the theory parameters, it is not sufficient to characterize the parameter uncertainty by means of a covariance matrix. Instead, these uncertainties must be provided as confidence intervals for the parameters.[1]

In the linear case, the confidence interval for an estimated parameter $\hat{a}$ is uniquely defined as the range of values within a distance corresponding to the parameter uncertainty $\hat{\sigma}_a$. This is suggested by the notation $\hat{a} \pm \hat{\sigma}_a$. For nonlinear problems, this interval is no longer centered around the best estimate $\hat{a}$, leading to asymmetric uncertainty estimates.

The notion corresponding to the confidence interval in terms of the multidimensional parameter space is that of the *confidence region*. In the linear case, it can be shown that this region corresponds to the ellipsoid centered around the best estimate $\hat{a}$ with the directions and lengths of the semi-axes given by the eigenvectors and eigenvalues of the parameter covariance matrix, respectively. For nonlinear problems, the ellipsoid becomes deformed.

However, in both the linear and nonlinear cases, this confidence region has the defining characteristic that the value of the χ^2 quantity at any point on its boundary corresponds to an increase of 1 with respect to the χ^2 value at its center. This enables numeric methods to be used for its determination.

In order to obtain confidence intervals for the parameters, a technique called *profiling* is commonly employed. Since the confidence interval is characterized by a unit increase in χ^2 with respect to the global minimum, the goal of this method is identifying the variation of the parameter being profiled corresponding to this increase.

To this end, the χ^2 quantity is evaluated as a function of the parameter being profiled, while performing a simultaneous minimization with respect to all other parameters. The values of the profiled parameter corresponding to a unit increase in χ^2 are quoted as the confidence interval for the parameter. Accordingly, this method is also called the "$\Delta\chi^2 = 1$ prescription".

In addition, parameter correlations may be determined by profiling two parameters simultaneously. The shape of the resulting confidence region in two-dimensional parameter space is indicative of the parameter correlation.

Offset Method

A considerably simpler method for the estimation of parameter uncertainties consists in applying a positive and negative offset to the measurements or theory predictions, the absolute value of which corresponds to the uncertainty in the quantity, and performing the χ^2 minimization again. The size of the spread observed in the best estimate for the parameters is taken to be the parameter uncertainty.

[1] In this work, the term *confidence interval* always refers to the Gaussian one-sigma confidence interval. This corresponds to a confidence level of approximately 68%.

This method has the advantage that is it comparatively easy to implement and provides an approximate estimate of the impact of a particular uncertainty on the estimated parameters. Unlike the previous methods, however, it provides no information about the correlation of theory parameters.

Nevertheless, in situations where the uncertainty is generated by the dependence of the measurement or of the theory on a particular external parameter which cannot be varied continuously, the offset method remains the only viable alternative. One particular example of an uncertainty which is typically estimated using the offset method is the uncertainty in fixed-order theoretical calculations resulting from the introduction of an additional dependence on the renormalization and factorization scales. While it is possible, in principle, for these to be varied, the resulting effect cannot be modeled using a Gaussian distribution. The associated "scale uncertainty" is therefore defined in terms of the effect of scale variations on the estimated parameters.

This uncertainty is conventionally derived in a so-called six-point scheme by applying multiplicative "offsets" of 2, 1, and 1/2 to the renormalization and factorization scales and repeating the χ^2 minimization. All combinations of factors are taken into account, with the exception of the extreme cases where one scale is set at half the nominal scale and the other is doubled (see, for example, [16]). The maximal deviations from the central result obtained for the nominal scales are quoted as the uncertainty.

4. Past Extractions of $\alpha_s(M_Z)$

The main focus of this thesis lies in achieving an extraction of the strong coupling constant $\alpha_s(M_Z)$ from a combined set of inclusive jet cross section measurements. In recent years, several such measurements have become available from various experimental collaborations at particle colliders such as HERA[1], the Tevatron[2], and the LHC[3].

In this thesis, such a combined extraction of $\alpha_s(M_Z)$ is approached using double differential measurements of the inclusive jet cross section from collider experiments at each of the above facilities, namely H1 at HERA, DØ at the Tevatron, and CMS at the LHC. Together, these measurements cover a large and complementary phase space, spanning over three orders of magnitude in transverse jet momentum. This offers a promising perspective for the study of QCD phenomenology.

A significant advantage of this choice of datasets for the combined extraction lies in the availability of past determinations of the strong coupling constant $\alpha_s(M_Z)$, which have been performed by the collaborations themselves. The original approaches serve as an important starting point in developing a common extraction procedure, as well as providing a direct means of comparing the methodology and results of the combined extraction to the original references.

In this chapter, a number of general aspects relating to inclusive jet cross section measurements, theory predictions, and the methodology of $\alpha_s(M_Z)$ determinations are discussed, followed by a review of the measurements and $\alpha_s(M_Z)$ determinations indicated above.

4.1. Jet Measurements and $\alpha_s(M_Z)$ Extractions at Hadron Colliders

Measurements of jet production cross sections in hadron-induced collisions at high energies provide an important experimental handle on phenomena governed by the strong interaction. In particular, they allow probing the validity of QCD predictions over an ample phase space, and contribute to a precise determination of fundamental QCD parameters such as the strong coupling constant $\alpha_s(M_Z)$.

In this respect, inclusive jet production cross sections are among the simplest observables, and can be measured in a number of elementary scattering processes. In the following, a number of measurements of inclusive jet cross sections in ep, pp, and $p\bar{p}$ scattering performed by the H1, DØ and CMS collaborations, respectively, are presented.

[1] *Hadron-Elektron-Ringanlage* ("Hadron-Electron Ring Accelerator"), a particle collider at DESY (*Deutsches Elektronen-Synchrotron*, "German Electron Synchrotron") in Hamburg, Germany
[2] A particle collider at Fermilab in Batavia, IL, USA
[3] The *Large Hadron Collider* at CERN (*European Organization for Nuclear Research*) in Geneva, Switzerland

4.1.1. Deep Inelastic Scattering at H1

One set of measurements of inclusive jet production in deep inelastic electron-proton scattering (ep) is available from the H1 experimental collaboration at HERA, along with a determination of $\alpha_s(M_Z)$ from these data. [17]

In deep inelastic ep scattering, jets are produced as a result of the interaction of color-charged particles in the proton scattering off the electron. Since leptons do not carry color charge, the hard scattering process is mediated by the exchange of a virtual electroweak boson, and thus is not directly sensitive to the strong coupling constant α_s at leading order in perturbation theory. Higher-order contributions to this process, however, become sensitive to α_s due to additional strong vertices in the corresponding Feynman diagrams.

In the above reference, double differential inclusive jet production cross sections are measured as a function of transverse jet momentum p_T and the boson virtuality Q^2, at a center-of-mass energy of $\sqrt{s} = 319\,\text{GeV}$. The data consist of 24 measurements, corresponding to different kinematic regions, with p_T ranging from 7 GeV to 50 GeV and Q^2 ranging from $150\,\text{GeV}^2$ to $15\,000\,\text{GeV}^2$.

Jet observables are reconstructed using both the k_T and the anti-k_T jet algorithms with a distance parameter of $R = 1$, yielding two distinct measurements. These are further processed using a regularized unfolding technique in order to correct for detector-related effects.

In addition to statistical fluctuations resulting from the limited sample size, a number of systematic experimental uncertainty sources are identified. One contribution to the total experimental uncertainty is due to the reconstruction of the hadronic final state. This uncertainty is subdivided into two separate contributions, one of which relates to the reconstruction of jets from hadronic objects, and the other accounting for the reconstruction of hadronic objects which are not clustered to jets.

For the reconstruction of the scattered lepton, uncertainties due to lepton identification, as well as the measurement of lepton energy and scattering angle are estimated.

An additional uncertainty source is introduced in order to account for uncertainties of the theoretical model. The magnitude of this effect is estimated by comparing the result of performing the unfolding procedure on both data and pseudodata with migration matrices obtained from different MC generators.

The normalization uncertainties resulting from the determination of the sample luminosity, as well as detector, reconstruction and trigger efficiencies, are taken as fully correlated across the entire measurement phase space. This also applies to the uncertainty generated by the algorithm for noise suppression in the liquid argon calorimeter.

All experimental uncertainties are propagated through the unfolding procedure in order to obtain uncertainty estimates for the unfolded measurements.

Theory predictions

Theory calculations of the inclusive jet cross section are performed at next-to-leading order in perturbation theory. In order to enable a fast recomputation of the theory

upon varying the value of $\alpha_s(M_Z)$, the fastNLO software package is used in conjunction with NLOJet++ (a detailed explanation of the fast calculation method is provided in section 5.1). The calculations are evaluated at a factorization scale identical to the boson virtuality Q, while the renormalization scale is chosen as:

$$\mu_R = \sqrt{\frac{Q^2 + {p_T}^2}{2}} \tag{4.1}$$

Here, p_T refers to the transverse momentum of the jet.

In order to account for hadronization effects, non-perturbative correction factors are calculated and applied to the predictions obtained in perturbative QCD. An estimation of hadronization effects is performed using the MC generators DJANGO [18] and RAPGAP [19], averaging the results obtained with the two generators for calculating the correction factor. A further correction factor due to electroweak radiative effects is estimated using the LEPTO event generator [20].

The data are compared to the theory predictions obtained for a number of global PDF sets, determined at NLO accuracy. These are the MSTW2008, CT10, NNPDF2.3, HERAPDF1.5 and ABM11 PDF sets. In general, the data are shown to be described well by the theory predictions obtained with all PDFs. Compared to the MSTW2008 and CT10 PDF sets, calculations with HERAPDF1.5 and ABM11 are seen to be consistently larger at low p_T, while falling below the predictions obtained for the other PDF sets at high transverse momenta.

Determination of $\alpha_s(M_Z)$

The value of the strong coupling constant $\alpha_s(M_Z)$ is determined from the measurement data using a least-squares estimation procedure. Determinations are performed for both sets of data obtained using the k_T and anti-k_T jet clustering algorithms.

The central estimate for $\alpha_s(M_Z)$ is obtained under consideration of the experimental uncertainties only. A number of assumptions are made for the correlations of these uncertainties. For statistical uncertainties, the full covariance matrix is derived. The uncertainties due to the reconstruction of hadronic objects are considered to have a correlation of 50% across all phase space regions, while normalization uncertainties are considered to be fully correlated. In contrast, the model and lepton reconstruction uncertainties are both considered to be uncorrelated across the different Q^2 bins, with the former assumed to be 25% correlated across the p_T bins, and the latter having a correlation of 100%.

For the estimation of $\alpha_s(M_Z)$, a χ^2 quantity to be minimized is defined under the assumption of a log-normal distribution for the measurements (see section 3.1.2). In

the nuisance parameter formulation, this quantity is defined as:

$$\chi^2_{\mathrm{H1}} = \mathbf{p}^\top \left({\mathbf{V}_{\mathrm{rel}}}^{-1} \right) \mathbf{p} + \sum_k^{N_{\mathrm{sys}}} {\varepsilon_k}^2 \tag{4.2}$$

Here, the matrix $\mathbf{V}_{\mathrm{rel}}$ is the sum of the relative covariance matrices corresponding to all experimental uncertainties, ε_k are the nuisance parameters representing fully correlated systematic effects, and $\mathbf{p}$ represents the agreement between the data $\mathbf{d}$ and the theory $\mathbf{t}$, which is defined for each data point by means of the logarithm of the ratio of their values:

$$p_i = \ln \frac{m_i}{t_i} + \sum_k^{N_{\mathrm{sys}}} E_i(\varepsilon_k) \tag{4.3}$$

In the above relation, the quantity $E_i(\varepsilon_k)$ represents the contribution to the observed measurement m_i caused by a systematic contribution due to the nuisance parameter ε_k. To allow for asymmetric effects, this quantity is defined using a second-degree polynomial interpolation of the uncertainties corresponding to the "up" and "down" variations of the respective measurement:

$$E_i(\varepsilon_k) = \sqrt{f_k^{\mathrm{Cor}}} \left(\frac{\delta_{m,i}^{k,\,\mathrm{up}} - \delta_{m,i}^{k,\,\mathrm{down}}}{2} \varepsilon_k + \frac{\delta_{m,i}^{k,\,\mathrm{up}} + \delta_{m,i}^{k,\,\mathrm{down}}}{2} {\varepsilon_k}^2 \right) \tag{4.4}$$

Here, f_k^{Cor} denotes the global correlation coefficient of the k-th uncertainty source. This allows partially correlated uncertainties to be split into a fully correlated part, handled via nuisance parameters, and an uncorrelated part, which is included in the covariance matrix.

After performing the minimization, the experimental uncertainty on $\alpha_s(M_Z)$ is estimated using linear uncertainty propagation. Uncertainties on the theory predictions due to the PDFs are estimated using the uncertainties provided for the MSTW2008 NLO PDF set, which uses the Hessian method outlined in [21]. The resulting eigenvector variations are found to be sufficiently symmetric and linearly propagated to estimate the PDF uncertainty on $\alpha_s(M_Z)$.

Similarly, the uncertainty on $\alpha_s(M_Z)$ resulting from applying non-perturbative correction factors accounting for hadronization, is also estimated by linearly propagating the theoretical uncertainties of the theory predictions. These are estimated using the SHERPA event generator [22] with both the Lund string and the cluster hadronization algorithms. Half the difference between the two resulting correction factors is taken to be the prediction uncertainty.

The uncertainties due to missing higher orders in perturbation theory are estimated separately for the cross section dependence on the renormalization and factorization scales. For this purpose, the theory predictions are computed for a continuous variation of each scale over an interval ranging from half the nominal scale to its double, taking the

maximum difference to the theory for the nominal scale as the associated uncertainty. The uncertainties on $\alpha_s(M_Z)$ are then obtained through linear propagation, assuming the scale dependence to be 50% correlated across all observable bins.

Finally, two additional uncertainty sources reflecting the choice of PDF set from among the available global PDF sets, as well as the choice of a PDF for a particular value of $\alpha_s(M_Z)$ within the PDF set, are estimated. This is achieved by performing additional fits with different PDF sets, and PDFs corresponding to different values of $\alpha_s(M_Z)$, respectively. Half the difference between the resulting estimates for $\alpha_s(M_Z)$ is quoted as the respective uncertainty.

The main result quoted for $\alpha_s(M_Z)$ is extracted from the measurements obtained using the k_T jet clustering algorithm. The central estimate for $\alpha_s(M_Z)$ and the uncertainties discussed above is given as:

$$\begin{aligned}\alpha_s(M_Z)_{\text{H1}} = 0.1174 &\pm 0.0022\ (\text{exp}) \pm 0.0007\ (\text{PDF}) \pm 0.0010\ (\text{had}) \\ &\pm 0.0007\ (\text{PDF set}) \pm 0.0005\ (\text{PDF } \alpha_s) \\ &\pm 0.0048\ (\mu_R) \pm 0.0006\ (\mu_F)\end{aligned} \tag{4.5}$$

An alternate estimate obtained from the anti-k_T data is found to be fully consistent with the k_T estimate.

4.1.2. Proton-Antiproton Scattering at DØ

At the Tevatron collider, measurements of inclusive jet production in $p\bar{p}$ scattering have been conducted. One such measurement, performed by the DØ experimental collaboration, [23] is reviewed here. In addition, a determination of the strong coupling constant $\alpha_s(M_Z)$ from these measurements has been performed, [24] which is also summarized here.

In contrast to deep inelastic scattering, jet production in $p\bar{p}$ scattering is sensitive to α_s at leading order in perturbation theory. The data collected by the DØ collaboration consist of double differential cross section measurements in transverse momentum p_T and jet rapidity y. The data points are organized into six bins of absolute jet rapidity $|y|$, ranging from 0.0 to 2.4, with a bin size of 0.4. For each absolute rapidity bin, the p_T binning varies, starting from transverse momenta of 50 GeV. Overall, the whole data set comprises 110 data points.

For the reconstruction of jet objects, an iterative cone-based algorithm relying on midpoint seeds, as described in [15], is used, with the cone radius set to $R = 0.7$. The measured properties of the jets are corrected for a number of systematic effects, such as the energy response of the detector. In addition, the effects of jet migration to neighboring bins on account of the finite detector resolution are estimated using a simulation of the DØ detector, and corrected by applying correction factors in each bin.

Statistical uncertainties on the cross section are estimated for each bin and taken to be uncorrelated. To account for experimental systematic effects, 24 uncertainty sources are introduced, of which 23 are taken to be fully correlated, while the remaining uncertainty source accounts for uncorrelated effects. The overall largest uncertainties are identified

to be due to the electromagnetic and photon energy scales.

For evaluating the measurement data, theory predictions are computed at next-to-leading order using the fastNLO framework in conjunction with the MRST2004 [25] and CTEQ6.5M [26] PDF sets. Non-perturbative correction factors are applied to account for hadronization and the underlying event. The corrected theory predictions are found to be in good agreement with the measurements.

Theory predictions

A determination of the strong coupling constant $\alpha_s(M_Z)$ from the above measurement is performed in a subsequent publication. [24] This is done following a least-squares approach by iterative minimization of a χ^2 quantity.

For this purpose, theory predictions are computed in the fastNLO framework using NLOJet++. Both the renormalization and factorization scales are identified with the transverse jet momentum p_T. The perturbative calculation is performed at next-to-leading order in pQCD and supplemented by threshold corrections computed to two-loop accuracy. [27] In the following, this is referred to as "approximate next-to-next-to-leading order" (aNNLO) calculation accuracy. The PDF set used is the global MSTW2008 NNLO PDF set.

In addition, non-perturbative correction factors due to hadronization and the underlying event, as estimated in the original measurement publication, are applied to the theory predictions.

In order to account for the implicit dependence of the resulting theory predictions on the value of $\alpha_s(M_Z)$ assumed when determining the PDFs, the calculations are performed for each PDF in the α_s series provided by the MSTW2008 NNLO PDF set. In order to obtain a continuous dependency of the cross section prediction on $\alpha_s(M_Z)$, the discrete cross section points thus obtained are interpolated using cubic splines.

Furthermore, a number of uncertainties on the theory are estimated, which are all taken as fully correlated across all data points. The uncertainties due to the PDFs are calculated from the eigenvector variations provided for the MSTW2008 NNLO PDF set using the Hessian approach. [21] In addition, for each non-perturbative correction factor applied to the perturbative calculation, an additional theory uncertainty corresponding to half the applied factor is estimated. An uncertainty due to the choice of scale is not estimated on the cross-section level.

Determination of $\alpha_s(M_Z)$

Since the above measurement is used in the MSTW2008 analysis to provide constraints on the PDFs, a number of data points which have a significant impact on the PDF determination are excluded from the $\alpha_s(M_Z)$ determination. The subset of the data used for the extraction of $\alpha_s(M_Z)$ thus contains only 22 of the original 110 data points.

In defining the χ^2 quantity, both experimental and theoretical uncertainties are taken into account. Of these, all systematic uncertainties except one are taken to be fully correlated across all data points and are included in the χ^2 definition as nuisance parameters.

No correlations between different observable bins are assumed for the statistical uncertainties.

While not explicitly documented in the publication, the exact mathematical expression for this quantity was kindly provided by the authors, and is given in (4.6).

$$\chi^2_{\mathrm{D\O}} = \sum_{i=1}^{N_{\mathrm{bins}}} \frac{\left[m_i - t_i \left(1 + \sum_{k=1}^{N_{\mathrm{sys}}^{\mathrm{theo}}} \delta_{ik}(\alpha_k)\right)\left(1 + \sum_{j=1}^{N_{\mathrm{sys}}^{\mathrm{exp}}} \delta_{ij}(\varepsilon_j)\right)^{-1}\right]^2}{{\sigma_{i,\,\mathrm{stat}}}^2 + {\sigma_{i,\,\mathrm{uncor}}}^2} + \sum_{j=1}^{N_{\mathrm{sys}}^{\mathrm{exp}}} {\varepsilon_j}^2 + \sum_{k=1}^{N_{\mathrm{sys}}^{\mathrm{theo}}} {\alpha_k}^2 \tag{4.6}$$

In the above relation, m_i and t_i refer to the measurement and theory prediction in the i-th observable bin, and $\sigma_{i,\,\mathrm{stat}}$ and $\sigma_{i,\,\mathrm{uncor}}$ refer to the statistical and uncorrelated systematic uncertainties. The theory prediction is weighted by factors resulting from contributions of the fully correlated experimental and theoretical systematic uncertainties. These are calculated as quadratic functions of the experimental and theoretical nuisance parameters (ε_j and α_k, respectively) by interpolating between the relative "up" and "down" uncertainty estimates:

$$\delta_{ij}(\varepsilon_j) = \left(\frac{\delta_{m,i}^{j,\,\mathrm{up}} - \delta_{m,i}^{j,\,\mathrm{down}}}{2} \varepsilon_j + \frac{\delta_{m,i}^{j,\,\mathrm{up}} + \delta_{m,i}^{j,\,\mathrm{down}}}{2} {\varepsilon_j}^2 \right) \tag{4.7}$$

A best estimate is extracted for $\alpha_s(M_Z)$ by performing a minimization of the χ^2 quantity (4.6), taking all experimental and theoretical uncertainties (except the scale uncertainty) into account. The uncertainties on the $\alpha_s(M_Z)$ estimate are estimated as one-sigma confidence intervals derived using the $\Delta\chi^2 = 1$ prescription.

In addition, the individual contributions to this uncertainty are estimated. These are contributions due to uncorrelated and correlated experimental effects, as well as due to non-perturbative, PDF and scale uncertainties. The latter are estimated by additional fits performed with both the renormalization and factorization scales set to half and double their nominal values. The differences of the resulting $\alpha_s(M_Z)$ estimates to the result obtained with the nominal scales are given as the scale uncertainty on $\alpha_s(M_Z)$. The exact method of estimation for the remaining contributions to the total uncertainty is not documented in the publication.

The central estimate for $\alpha_s(M_Z)$, as well as the uncertainty contributions, are determined at aNNLO using the method summarized above and are given as:

$$\begin{aligned}\alpha_s(M_Z)_{\mathrm{D\O,\,aNNLO}} = 0.1161 \pm 0.0001\ (\mathrm{exp,uncor})\ {}^{+0.0034}_{-0.0033}\ (\mathrm{exp,cor}) \\ {}^{+0.0010}_{-0.0016}\ (\mathrm{NP})\ {}^{+0.0011}_{-0.0012}\ (\mathrm{PDF})\ {}^{+0.0025}_{-0.0029}\ (\mathrm{scale})\end{aligned} \tag{4.8}$$

In addition, the result of a determination using the calculations performed at NLO without the inclusion of threshold corrections, as well as NLO PDFs, is provided. For

this result, only an estimate of the total uncertainty is quoted:

$$\alpha_s(M_Z)_{\mathrm{D\O,\,NLO}} = 0.1202\ ^{+0.0053}_{-0.0024}\ (\mathrm{total}) \tag{4.9}$$

4.1.3. Proton-Proton Scattering at CMS

Inclusive jet production has also been measured in pp collisions at the LHC. In the following, one such measurement conducted by the CMS experimental collaboration at a center of mass energy of 7 TeV [28] is reviewed. These data have been used for a determination of the strong coupling constant by the CMS experimental collaboration. [29]

During the 2011 run of the LHC, inclusive jet production cross sections have been measured by the CMS experimental collaboration in pp collisions at a center-of-mass energy of 7 TeV. The collected data consist of double differential inclusive jet cross sections, measured as a function of transverse jet momentum p_T and jet rapidity y. The measurement phase space is divided into five equally-sized bins of absolute jet rapidity $|y|$, ranging from 0.0 to 2.5. In each absolute rapidity bin, the p_T phase space is subdivided into a variable number of bins with a bin size proportional to the p_T resolution, starting at $p_T = 114\,\mathrm{GeV}$. In total, the dataset consists of 133 data points.

The reconstruction of jet objects is performed using the anti-k_T jet algorithm with a distance parameter of $R = 0.7$, and involves a number of corrections due to systematic effects, such as detector and reconstruction inefficiencies, or additional pp interactions. In addition, the data are unfolded in order to account for event migration between bins due to the detector resolution. The magnitude of the corrections, as well as the migration matrix used for the unfolding procedure, are obtained from Monte Carlo studies in conjunction with simulations of the CMS detector.

A number of experimental uncertainties are estimated in order to account for statistical fluctuations and systematic effects on the measurements. The dominant sources of systematic uncertainty are identified to be due to the jet energy scale, the luminosity and the resolution of jet p_T. The jet energy scale uncertainty is described by means of 16 mutually uncorrelated contributions, each of which is taken to be fully correlated across the entire measurement phase space.

The luminosity uncertainty on the measured cross section is estimated to be 2.2%, equally affecting all observable bins. An additional uncertainty due to the unfolding procedure is estimated to be of the order of 3–4%, and is assumed to be fully correlated across all p_T bins. Remaining uncorrelated systematic effects are accounted for by an additional uncertainty of 1%.

Theory predictions

For the purpose of determining $\alpha_s(M_Z)$, next-to-leading order calculations of the cross section are performed with the fastNLO framework in conjunction with the NLOJet++ software package. The calculations are performed with the values for the renormalization and factorization scales being identified with the transverse momentum of the individual jets. Predictions are obtained for the ABM11, CT10, MSTW2008 and NNPDF2.1

NLO PDF sets.

In addition, the calculations are corrected using non-perturbative factors in order to account for multiple-parton interactions and hadronization effects. The correction factors are calculated using three separate calculation setups. One set of calculations is performed with the POWHEG package, [30] with matched parton showering and hadronization performed with the Pythia 6 event generator. [31] Another set of calculations is performed with Pythia 6 alone, and a third using Herwig++. [32] The center of the envelope given by all three calculations is chosen as the non-perturbative correction factor. Furthermore, electroweak radiative effects are also accounted for by means of correction factors. [33]

Finally, the uncertainties on the theory are estimated. The uncertainty on the theory resulting from the PDF determination is estimated for each PDF set and provided as a covariance matrix. This is done both for PDF sets providing eigenvector variations, in which case the Hessian method [21] is used, as well as NNPDF2.1, which provides a statistical ensemble of Monte Carlo replicas. In the latter case, these ensembles are used to estimate the covariance matrix of the predictions directly. In addition, an uncertainty is introduced due to the non-perturbative corrections. It is estimated as half the spread between the three sets of theory calculations performed.

Determination of $\alpha_s(M_Z)$

An extraction of $\alpha_s(M_Z)$ from the inclusive jet measurement is performed using an approach based on least-squares estimation. However, in contrast to the traditional procedure involving the direct iterative minimization of a χ^2 quantity with respect to the theory parameter $\alpha_s(M_Z)$, an method of estimation based on the calculation of the χ^2 quantity for a discrete number of $\alpha_s(M_Z)$ points is employed.

This is done in order to account for the dependence of the PDFs used for the calculation on the value of $\alpha_s(M_Z)$ assumed for their determination. Since the global PDFs provided as part of an α_s series are only available for discrete values of $\alpha_s(M_Z)$, the χ^2 quantity is only evaluated at these points, using the corresponding PDF in the α_s series for each evaluation. In order to obtain a continuous χ^2 function, a second-degree polynomial is fitted to the resulting $\left(\alpha_s(M_Z), \chi^2\right)$ points.

All experimental uncertainties, as well as PDF uncertainties, are considered in evaluating the χ^2 quantity. However, a number of studies performed reveal the need of adjusting the correlation model presented in the original measurement publication. The adjustment concerns the uncertainty correlations related to the single-particle response jet energy corrections.

To determine an improved model for the correlation, the original assumption of a full correlation of this uncertainty across all absolute rapidity bins is evaluated by performing separate determinations of $\alpha_s(M_Z)$ in each individual bin, as well as for all bins with different assumptions for the correlation in $|y|$. On account of the poor fit quality when assuming a correlation of 100%, the correlation model is revised. For the $\alpha_s(M_Z)$ determination, the single-particle response uncertainty is taken to be uncorrelated between the barrel ($|y| < 1.5$) and endcap ($1.5 \leq |y| < 2.5$) detector regions, while continuing to

exhibit correlations of 50% in the former region and 100% in the latter.

The definition of the χ^2 quantity is defined as:

$$\chi^2_{\text{CMS}} = (\mathbf{m} - \mathbf{t})^\top \left(\mathbf{V}^{-1}\right) (\mathbf{m} - \mathbf{t}) \tag{4.10}$$

Here, $\mathbf{m}$ and $\mathbf{t}$ refer to the measurement and theory predictions, and the covariance matrix $\mathbf{V}$ is the sum of the covariance matrices accounting for the statistical and uncorrelated systematic uncertainties, the luminosity uncertainty, the uncertainties due to the jet energy scale and unfolding, as well as the PDF uncertainties.

Best estimates for $\alpha_s(M_Z)$ are obtained by determining the minimum of the parabola fitted to the χ^2 points for the different discrete $\alpha_s(M_Z)$ points, while the total uncertainty on $\alpha_s(M_Z)$ due to experimental effects and PDFs is estimated as a confidence interval by applying the $\Delta\chi^2 = 1$ prescription. Separate estimates for the experimental and PDF uncertainties on $\alpha_s(M_Z)$ are obtained by repeating the estimation without the inclusion of the PDF covariance matrix in (4.10). The resulting uncertainty estimate is taken to be the experimental uncertainty on $\alpha_s(M_Z)$, and an estimate for the PDF uncertainty is obtained by subtracting the experimental uncertainty from the total uncertainty in quadrature.

An additional uncertainty on $\alpha_s(M_Z)$ due to non-perturbative effects is estimated by repeating the extraction with a variation of the theory predictions corresponding to the size of the non-perturbative uncertainty. The maximal deviation from the central estimate for $\alpha_s(M_Z)$ is taken as the uncertainty value.

Finally, the uncertainty due to the renormalization and factorization scales is estimated in a similar fashion, following the conventional six-point variation of the scale choices. An asymmetric uncertainty is derived from the maximal resulting upward and downward variations in the estimate for $\alpha_s(M_Z)$.

Extractions of $\alpha_s(M_Z)$ are performed with the CT10, MSTW2008 and NNPDF2.1 NLO PDF sets. No determination is performed with the ABM11 PDF set due to a significant difference in shape seen for the theory predictions obtained with this PDF set compared to both the measurement and the predictions derived using other PDF sets.

The final result of the extraction is quoted for the CT10 PDF set as:

$$\alpha_s(M_Z)_{\text{CMS}} = 0.1185 \pm 0.0019\ (\text{exp}) \pm 0.0028\ (\text{PDF}) \pm 0.0004\ (\text{NP}) \,{}^{+0.0053}_{-0.0024}\ (\text{scale}) \tag{4.11}$$

4.2. Conclusion

In this chapter, a presentation of the inclusive jet cross section measurements and the associated extractions of $\alpha_s(M_Z)$ performed by the H1, DØ and CMS experimental collaborations is given.

A comparison of these measurements and $\alpha_s(M_Z)$ determinations reveals a number of significant differences. One difference concerns the experimental techniques used for the measurement, as well as the estimation of the experimental uncertainties and their correlations. In part, these differences are a natural consequence of the experimental setup, which is unique to each individual experiment. A number of differences,

however, such as the employed jet clustering algorithm, are due to choices made by the experimental collaborations.

Furthermore, a number of differences can be observed concerning the theory calculations employed for the extractions of $\alpha_s(M_Z)$, with the individual experimental collaborations making use of different software tools for performing pQCD calculations. The identification and calculation of non-perturbative correction factors to the perturbative QCD calculations is also performed differently in each approach.

Finally, among the largest differences between the determination of $\alpha_s(M_Z)$ performed by the different collaborations lies in the extraction methodology itself. The main difference here concerns the method of accounting for the implicit dependence of PDFs on the value of $\alpha_s(M_Z)$ assumed for their determination, for which each collaboration takes a different approach. In addition, the treatment of uncertainties on the measurement data, as well as the theory predictions, is observed to vary significantly between the different approaches. This is also reflected in the definition of a χ^2 quantity, where a different choice is made by each of the collaborations. Similarly, a number of differences can be identified concerning the estimation of uncertainties on the final estimate of $\alpha_s(M_Z)$ quoted by the collaborations.

In light of the differences in methodology outlined above, the need for developing a unified procedure for the extraction of the strong coupling constant $\alpha_s(M_Z)$ from a combined dataset of the above measurements becomes clear. A discussion of several aspects relevant for the development of such a method, as well as the resulting unified extraction procedure, is provided in chapter 6.

5. Software Tools

For the development and technical implementation of the $\alpha_s(M_Z)$ determination, a number of software tools are employed. These provide the necessary functionality for computing theory predictions for observables as a function of the theory parameters, as well as access to statistical and other numerical routines used in parameter estimation. In this section, the functionality of a number of these tools is reviewed.

An essential component in iterative determinations of $\alpha_s(M_Z)$ is the fast calculation of theory predictions as a function of QCD-related parameters. This is provided by the fastNLO package. Also important in conjunction with $\alpha_s(M_Z)$ extractions is the ability to study the estimates obtained with several global PDFs. To this end, an interface providing standardized access to PDFs is required. This is provided by the LHAPDF 6 software package.

Finally, the extraction procedure is implemented in Alpos, a C++ framework for data-to-theory comparison and fitting. An overview of the functionality offered by Alpos is provided in section section 5.3, with particular emphasis on determinations of $\alpha_s(M_Z)$.

5.1. fastNLO

Cross section predictions for hadronic particle collisions involve a convolution of the hard scattering cross section with the parton distribution functions (PDFs) of the colliding hadrons (2.14). Whereas the PDFs are typically available as parametrized functions of the momentum fraction x and the energy scale Q, the hard scattering cross section must be calculated in perturbative QCD using Monte Carlo (MC) techniques.

This is generally a time-consuming process. For instance, fixed-order jet cross section calculations performed at next-to-leading-order (NLO) accuracy with the MC cross section integrator NLOJet++ [34, 35] require a computing time of several thousand CPU hours on modern architectures. In the absence of optimization techniques to reduce the calculation complexity, this limits the ability to further process these calculations.

The complexity of full NLO calculations is particularly prohibitive for iterative parameter estimation, which requires rapid recomputation of the theory predictions under a variation of the theory parameters. The fastNLO package [36] addresses this limitation, providing a fast and accurate means of calculating fixed-order hadronic cross section predictions beyond leading order, and thus allowing them to be used efficiently in studies of PDFs and the strong coupling constant. This section reviews the basic principle of optimization used by fastNLO.

5.1.1. Calculation Method

Computations of cross section predictions for hadronic processes involve a convolution of the partonic perturbation coefficients and the parton distribution functions with respect to the momentum fractions x_1 and x_2 of the participating partons. The convolution appears as a double integral over the momentum fractions and can be evaluated using Monte Carlo integration.

This calculation is particularly time-consuming due to the necessity of recalculating the perturbative coefficients for randomly sampled x_1 and x_2. Furthermore, the convolution result depends on the particular PDF set, meaning that it must be recomputed whenever the PDF changes.

Nevertheless, since the integrand factorizes, it is possible to take advantage of this for obtaining a PDF-independent representation of the convolution result. This section discusses such an approach, implemented by the fastNLO package.

As a starting point, we consider the expression for a fixed order calculation of the hadronic cross section:

$$\sigma_{\mathrm{pp}} = \sum_{p=0}^{P} \sum_{k=1}^{K} {\alpha_{\mathrm{s}}}^{p}(\mu_{\mathrm{R}}) \int \mathrm{d}x_1 \, \mathrm{d}x_2 \;\; c_k^{(p)}(x_1, x_2, \mu_{\mathrm{R}}, \mu_{\mathrm{F}}) \;\; F_k(x_1, x_2, \mu_{\mathrm{F}}) \tag{5.1}$$

To maintain simplicity, we express the PDF dependence in terms of a finite number of K linear combinations of parton flavors, which we denote $F_k(x_1, x_2, \mu_{\mathrm{F}})$, with the index k running from 1 to K. Additionally, we indicate the α_{s} dependence and the perturbative coefficients explicitly. There is one such coefficient $c_k^{(p)}$ for each order p in perturbation theory, and each parton flavor combination k.

It can be seen from (5.1) that evaluating the convolution integral requires knowledge of both the perturbative coefficient $c_k^{(p)}$ and the PDFs F_k at the time of computation. To achieve a PDF-independent representation, fastNLO employs an interpolation procedure, which is outlined below.

We first limit our discussion to factorizing the x-dependence of the PDFs. By evaluating $c_k^{(p)}(x_1, x_2)$ and $F_k(x_1, x_2)$ on a lattice given by a fixed set of points $\left\{x_1^{(i)}\right\}$ and $\left\{x_2^{(j)}\right\}$, the expression under the integral in (5.1) may be approximated as:

$$F_k(x_1, x_2) = \left[\sum_{ij} F_k\left(x_1^{(i)}, x_2^{(j)}\right) \right] I^{(i)}(x_1) \, I^{(j)}(x_2) \tag{5.2}$$

Here, $I^{(i)}(x_1)$ and $I^{(j)}(x_2)$ denote the interpolation functions corresponding to the i-th and j-th support points $x_1^{(i)}$ and $x_2^{(j)}$, respectively. Also note that there remains an implicit dependence on the renormalization and factorization scales, which we omit for notational simplicity. As can be seen from (5.2), once the support points in x_1 and x_2 have been chosen, the expression in brackets is a constant which no longer depends on the convolution variables x_1 and x_2. Thus, the convolution may be carried out independently of the PDFs by performing the convolution integration in (5.1) for a chosen set of

interpolation functions:

$$\int \mathrm{d}x_1\,\mathrm{d}x_2\;\; c_k^{(p)}(x_1,x_2)\;\; F_k(x_1,x_2) = \sum_{ij}\left[\int \mathrm{d}x_1\,\mathrm{d}x_2\;\; c_k^{(p)}(x_1,x_2)\;\; I^{(i)}(x_1)\,I^{(j)}(x_2)\right]\;\; F_k\left(x_1^{(i)},x_2^{(j)}\right) \tag{5.3}$$

In the above formula, the convolution has been reduced to a sum where the PDF dependence has been factorized out from each term. The expression in brackets only depends on the indices i, j, k and the order p in perturbation theory. Consequently, it may be computed numerically via Monte Carlo integration without explicit knowledge of the PDFs and stored in lookup tables for fast access.

The above reasoning may be extended to include the renormalization and factorization scales by also evaluating the relevant quantities at fixed values of μ_R and μ_F and performing an interpolation in each. Denoting the additional dimensions of the lookup table by the indices r and f, respectively, we obtain an analog of the expression in brackets in (5.3):

$$\tilde{\sigma}_{ijrf}^{(p)}(\mu_\mathrm{R},\mu_\mathrm{F}) = \int \mathrm{d}x_1\,\mathrm{d}x_2\; c_k^{(p)}(x_1,x_2,\mu_\mathrm{R},\mu_\mathrm{F})\;\; I^{(i)}(x_1)\,I^{(j)}(x_2)\,I^{(r)}(\mu_\mathrm{R})\,I^{(f)}(\mu_\mathrm{F}) \tag{5.4}$$

The quantity defined above encodes all the relevant information for calculating the final cross section at arbitrary scales within the interpolation region, with the exception of the PDF and α_s-dependent parts of the calculation. These are reintroduced by appropriate sums over the interpolation indices in order to obtain the final cross section:

$$\sigma_\mathrm{pp}(\mu_\mathrm{R},\mu_\mathrm{F}) = \sum_{p=0}^{P}\sum_{ijrf}\;\; \tilde{\sigma}_{ijrf}^{(p)}(\mu_\mathrm{R},\mu_\mathrm{F})\;\; {\alpha_\mathrm{s}}^p\left({\mu_\mathrm{R}}^{(r)}\right)\;\; F_k\left(x_1^{(i)},x_2^{(j)},{\mu_\mathrm{R}}^{(r)},{\mu_\mathrm{F}}^{(f)}\right) \tag{5.5}$$

An advantage of this procedure is the factorization of the calculation into a part which depends on the PDFs and α_s, and a universal part, which only depends on the chosen interpolation functions and coefficients.

Thus, a fastNLO table may be used for rapid recomputation of theory predictions under a change or variations of α_s, the PDFs and the renormalization and factorization scales. This allows these dependencies to be studied in data-theory comparisons and parameter estimation procedures. Such fastNLO tables have been computed and are available for all measurements discussed in this work.

Naturally, as with any interpolation method, the cross section predictions performed with fastNLO are only an approximation of the full calculations. As such, the question of accuracy arises. For an appropriately chosen number of points for the x and $\mu_\mathrm{R,F}$ interpolations, the difference between the full calculation and the results obtained by the interpolation method is below 0.1%. [36]

5.2. LHAPDF

Parton distribution functions indicate the probability density of a parton carrying a fraction x of the total hadron momentum at a particular factorization scale μ_F. Whereas the μ_F dependency can be derived from the DGLAP evolution equations (2.13), the x dependency needs to be parametrized. This allows PDFs to be uniquely represented by their respective parameters.

However, since PDFs can be parametrized in a number of different ways, this representation is not unique and may be chosen freely, subject to a number of reasonable restrictions, such as requiring the parton density to approach zero near the elastic threshold at $x = 1$.

In addition to employing different parametrizations, groups specializing in the determination of PDFs also make different choices regarding the experimental data considered for the fits, as well as applying different fitting procedures and conventions for representing the resulting uncertainties. Possible insights may be gained from comparing different global PDF sets, marking the need for standardized interfaces for accessing PDFs.

One such interface is LHAPDF 6, [37] a C++ library providing access to a large number of PDFs, as well as implementing several routines for performing PDF-related tasks, such as the estimation of PDF uncertainties.

5.3. The Alpos Data-to-Theory Comparison and Fitting Framework

Alpos [38] is a C++ software package providing a wide range of functionality for performing data-to-theory comparisons and parameter estimation. Among the main features of Alpos are an object-oriented and modular structure, the availability of interfaces to a large number of theory tools, as well as the implementation of fast numerical techniques, complemented by appropriate caching strategies in order to increase efficiency.

A core aspect specifically addressed by Alpos is the management of the dependencies between the parameters entering different theory calculations in an efficient and consistent manner. In addition, Alpos allows fine-grained control over the definition of an uncertainty model for the measurements and theory predictions, as well offering multiple definitions for χ^2 quantities to be used for parameter estimation.

In the following, an overview of the structure of the Alpos package is provided, with particular emphasis placed on the implementation of $\alpha_s(M_Z)$ determinations within this framework.

5.3.1. Package Structure

The main purpose of Alpos is to provide the necessary functionality for the comparison of measurement data to theory predictions, as well as the estimation of theory parameters. Consequently, a core feature of Alpos are the specialized data structures necessary for representing the measurement data and the corresponding theory predictions. In

order to enable the evaluation of theory computations as a function of physical and technical parameters, a number of interfaces to external packages are implemented.

In Alpos, an object-oriented approach is taken. The different components relevant for data-to-theory comparisons are represented by specialized objects. For instance, the individual theory parameters are represented by objects storing their current value as a data member and providing methods for obtaining, modifying and updating this value.

Objects representing the theory calculations provide methods for computing and storing the predicted values for the corresponding measurements as a function of the current values of the theory parameters. Furthermore, objects representing the measurement datasets store both the measurement values and associated metadata, such as the phase space covered by the observable bins.

A representation of the measurement and theory uncertainties is provided by dedicated objects, stored as data members of the objects to which they refer. These objects provide access to various representations of uncertainties, such as absolute and relative binwise uncertainties, or covariance and correlation matrices.

In Alpos, the central tool for workflow specification is the *task*. Each task implements a particular workflow element, such as the statistical analysis of the data-theory agreement, or the estimation of theory parameters from measurements using the least-squares method. The implementation of complex analysis procedures can thus be realized as a series of tasks.

User input is provided in the form of so-called *steering files*, which contain the necessary specifications required to run an analysis. Information regarding the measurement datasets and theory calculations, as well as the tasks to be executed, is provided by means of this file.

By making extensive use of class inheritance, a high degree of flexibility in working with these objects is achieved. In addition, the implementation of well-known design patterns, such as *caching*, *lazy evaluation*, and the *observer pattern* for notifying dependent objects of changes, contribute to computational efficiency and consistency.

Finally, the modular design of Alpos promotes extensibility, enabling further functionality to be implemented, such as new tasks or additional interfaces to external theory programs. An overview of the class hierarchy of Alpos is shown in figure 5.1.

5.3.2. Determination of $\alpha_s(M_Z)$ in Alpos

Alpos provides all the necessary components for performing determinations of the strong coupling constant $\alpha_s(M_Z)$ from measurement data. Furthermore, it allows a high degree of control over the essential elements of such a determination.

A central element consists of the measurement data itself. In Alpos, these data are provided as static *datafiles* containing the measurements in a plain text tabular format. The data table contains one row per observable bin and at lease An arbitrary number of additional columns can be specified for providing phase space information, as well as binwise uncertainties and multiplicative correction factors.

In addition, the datafiles contain a representation of the uncertainty model. For this, a number of uncertainty sources can be specified in a plain text tabular format. The

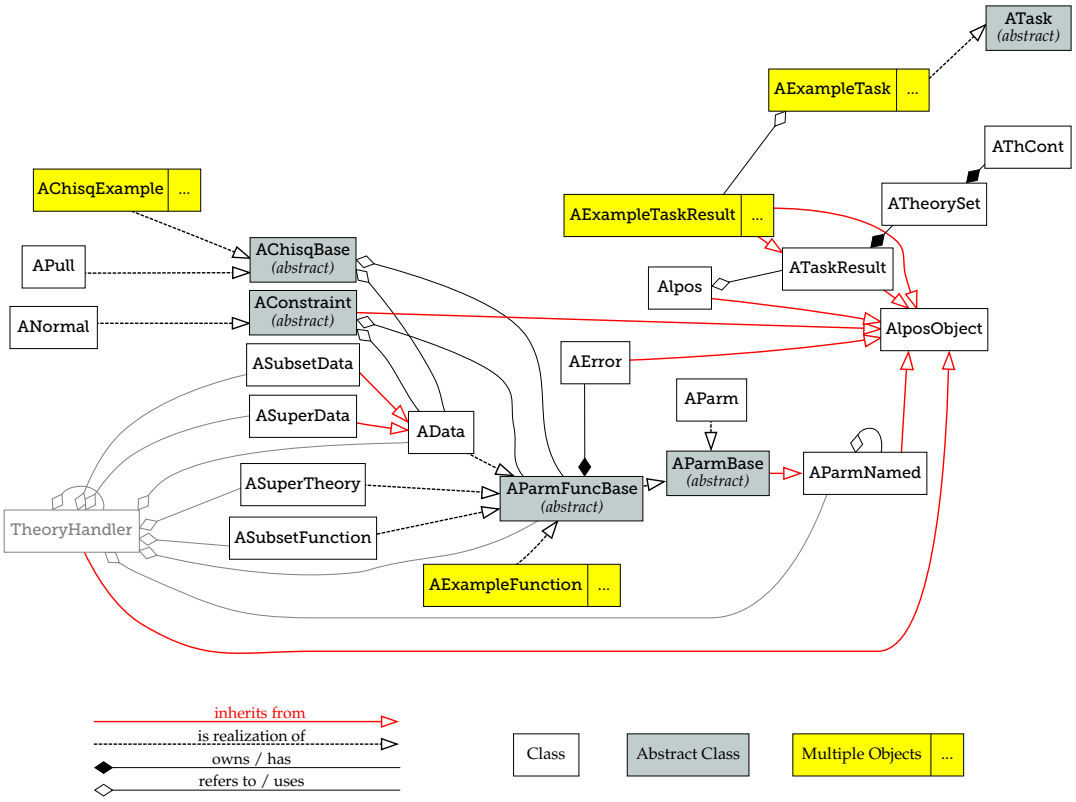

Figure 5.1.: Dependency structure of Alpos classes. The nodes shown in yellow each represent a collection of classes representing theory interfaces, χ^2 definitions, or Alpos tasks and task results. For each category of objects, a public interface is defined in the abstract parent class, allowing advanced users to implement additional functionality.

uncertainty is provided either as a reference to a particular column in the data table, indicating the magnitude of the uncertainty in a particular bin, or by directly specifying a number as the uncertainty in all observable bins. Asymmetric uncertainties are specified by providing two columns (or numbers), indicating the "up" and "down" uncertainties.

To provide additional information about the desired treatment of the uncertainties during parameter estimation, each uncertainty source is marked using a series of flags. These are used to distinguish uncertainties on the measurement from theory uncertainties, and statistical uncertainties from systematic ones. Additive and multiplicative uncertainty sources may also be specified in this way. In addition, bin-to-bin correlations for the different uncertainty sources can be specified by providing either a global correlation coefficient or a correlation matrix.

A further highlight of Alpos is the incorporation of interfaces to different programs for computing theory predictions. In this work, the theory calculations for inclusive jet cross

sections are provided by means of fastNLO interpolation tables. These are specific to each dataset and can be loaded in Alpos for providing the corresponding theory predictions as a function of $\alpha_s(M_Z)$. PDFs are also provided in Alpos by an interface to LHAPDF 6 and an interface to the CRunDec [39] package exists for the evolution of α_s to different energy scales.

The final prerequisite for a determination of $\alpha_s(M_Z)$ consists in establishing a definition of the χ^2 quantity to be minimized. Several χ^2 definitions are available in Alpos. The minimization with respect to $\alpha_s(M_Z)$ is performed numerically using the function minimizer MINUIT from the data analysis framework ROOT [40].

6. Extraction of $\alpha_s(M_Z)$ from the Combined Datasets

As described in chapter 4, extractions of the strong coupling constant $\alpha_s(M_Z)$ from inclusive jet measurements have been performed by several experimental collaborations, each using a characteristic extraction method. The main focus of this work is the determination of the strong coupling constant from inclusive jet measurements performed at multiple experiments.

Naturally, this type of extraction requires a consistent treatment of the measurement data, the corresponding theory predictions, and the different uncertainty models, in order to develop a unified fitting procedure. This enables the datasets to be compared on an equal footing and more precise estimates for $\alpha_s(M_Z)$ to be obtained.

In this work, such an extraction of the strong coupling constant is performed using the Alpos framework presented in section 5.3. As a means of verifying the functionality of Alpos in the context of determinations of α_s, a first aim is implementing the analyses outlined in chapter 4 within this framework. This is presented in section 6.1.

Having reproduced the original analyses, the next step towards a combined extraction of $\alpha_s(M_Z)$ is the definition of a unified fitting procedure which can be applied to all datasets. This includes choosing a suitable definition of a χ^2-like quantity for describing the data-theory agreement. For this purpose, it is important both to establish a consistent, robust manner of treating various systematic uncertainties, and to provide an exact specification of the necessary components entering the calculation of theory predictions. This procedure is presented in detail in section 6.2.

Subsequently, the unified fitting procedure is applied to the original datasets individually, and the results are compared to the respective original fitting procedures (section 6.3). This comparison is useful for understanding the strengths and weaknesses of each method, as it applies to the problem at hand.

Finally, the unified fitting procedure is applied to the combined dataset consisting of measurements from all three experiments, yielding the final value of $\alpha_s(M_Z)$ (section 6.4).

6.1. Reproduction of Past Determinations of $\alpha_s(M_Z)$

In chapter 4, past determinations of $\alpha_s(M_Z)$ by the H1, DØ and CMS collaborations have been reviewed. Each of these extractions employs a unique fitting procedure, which is described in the respective publications. Since the object of this work is a combined extraction of $\alpha_s(M_Z)$ in Alpos, a sensible first step is the reproduction of previous fit results within this framework. This serves as an important initial cross-check, ensuring

an understanding of the original datasets and fitting procedures, and as a demonstration of the functionality range and flexibility of Alpos for performing $\alpha_s(M_Z)$ extractions.

For this purpose, the main focus lies in reproducing the central estimate for $\alpha_s(M_Z)$ quoted by each collaboration, as well as the associated experimental uncertainty. On account of the extractions exhibiting significant procedural differences in the estimation of other contributions to the total uncertainty on $\alpha_s(M_Z)$, these are not estimated in the reproduction.

In the H1 fitting procedure, the central estimate for $\alpha_s(M_Z)$ is obtained by iterative minimization of the χ^2 quantity defined by taking only experimental errors into account. The DØ collaboration also performs an iterative χ^2 minimization. However, in contrast to H1, the χ^2 definition for estimating the central value of $\alpha_s(M_Z)$ also includes PDF uncertainties and uncertainties due to non-perturbative corrections. The experimental contributions to the resulting total uncertainties are obtained by performing additional fits, as described in section 4.1.

The extraction performed by CMS obtains estimates for $\alpha_s(M_Z)$ by evaluating the χ^2 quantity for a discrete number of $\alpha_s(M_Z)$ points and fitting a second-degree polynomial (see section 4.1.3). The central value of $\alpha_s(M_Z)$ is given by the location of the function minimum, and the uncertainty is evaluated according to the $\Delta\chi^2 = 1$ prescription, as described in section 3.3.

The three methods outlined can be implemented in Alpos and reproduce the original estimates for $\alpha_s(M_Z)$ exactly (up to rounding). A summary of the original estimates and the corresponding reproductions with Alpos can be found in table 6.1, and a visual representation of these results is shown in figure 6.1.

For the DØ analysis, both $\alpha_s(M_Z)$ extractions performed at NLO and at aNNLO accuracy are reproduced. Whereas central values and total uncertainties are provided in the publication, a detailed documentation of the various uncertainty components is only available for the aNNLO determination. Thus, the experimental uncertainties estimated with Alpos can only be compared to the original publication values for the aNNLO extraction.

The reproduced experimental uncertainties also correspond to the originally quoted estimates in almost all cases. A slight discrepancy can be seen for the reproduction of the DØ experimental uncertainty, which could be explained by numerical effects. Additionally, since the exact method of estimating the individual uncertainty contributions is not elaborated upon in the original publication, a slight procedural difference may be responsible for the discrepancy. Nevertheless, the exact reproduction of the central value is a strong indication of a correct reproduction.

Overall, the ability to implement different fit methodologies in Alpos, as well as the ability to reproduce published results, demonstrate the flexibility and suitability of the framework for determinations of $\alpha_s(M_Z)$ in general.

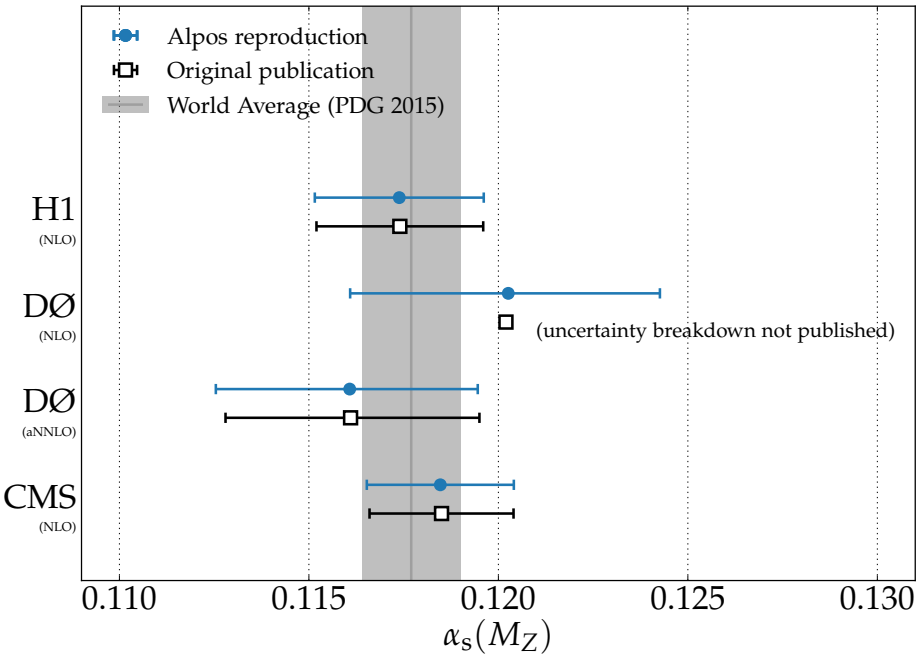

Figure 6.1.: Reproduction of past determinations of $\alpha_s(M_Z)$ by the H1, DØ and CMS collaborations with Alpos. The obtained values for $\alpha_s(M_Z)$ are shown here with error bars corresponding to the experimental uncertainty. The results obtained with Alpos are identical to those from the original publications. Also shown is the world average for α_s quoted in [12].

6.2. Unified Fitting Procedure

The fitting procedures outlined in chapter 4 and in the preceding section differ significantly. Thus, in order to perform a determination of $\alpha_s(M_Z)$ taking into account all datasets simultaneously, a new, unified fitting procedure must be developed.

One main point of difference among the original fitting procedures is the handling of the theory predictions. In order to ensure a consistent treatment of the theory, the order in perturbation theory for all calculations performed in the unified fitting procedure is required to be the same for each dataset. In this analysis, the calculations are performed at next-to-leading order accuracy.

Furthermore, the original procedures differ in their treatment of PDFs. The main difference lies in handling the dependence of PDFs on the strong coupling constant $\alpha_s(M_Z)$. Since PDFs play an important part in the calculation of the theory predictions used in determinations of $\alpha_s(M_Z)$, accounting for this dependence is a crucial part of ensuring an accurate and consistent treatment of the theory.

Another necessity of the unified fitting procedure is the establishment of an uncer-

		Central value	**Experimental uncertainty**		
		$\alpha_s(M_Z)$	$\pm\langle value\rangle$		(symmetric)
			$\langle down\rangle$	$\langle up\rangle$	(asymmetric)
H1	Publication	0.1174	$\pm$0.0022		
	Alpos	0.11739	$\pm$0.00223		
DØ (aNNLO)	Publication	0.1161	-0.0033	$+0.0034$	
	Alpos	0.11608	$-0.00353^{\dagger}$	$+0.00338$	
CMS	Publication	0.1185	$\pm$0.0019		
	Alpos	0.11847	$\pm$0.00194		

Table 6.1.: Comparison of the original fit results and the Alpos reproduction. Alpos results are given to a higher numerical precision in order to illustrate the impact of rounding. Overall, both central values and experimental uncertainties obtained with Alpos are in good numerical agreement with the original publication values. The slight discrepancy seen for the DØ asymmetric 'down' uncertainty (†) may be due to numerical effects.

tainty model for the measurements and the theory predictions. This aspect, as well as its implications for the definition of a χ^2 quantity, are also discussed.

Finally, the uncertainty on the final estimate obtained for $\alpha_s(M_Z)$ is estimated and the individual contributions to this uncertainty are quantified.

6.2.1. Implicit Dependence of PDFs on $\alpha_s(M_Z)$

Apart from the strong coupling constant $\alpha_s(M_Z)$, PDFs are a central component in theoretical calculations of jet cross sections. Since PDFs are determined by fitting theory predictions to experimental data, the value of $\alpha_s(M_Z)$ used for the theoretical calculations must either be determined alongside the PDF parameters, or remain fixed to a particular value during the PDF fit. Thus, each PDF determined in this manner has an associated value of $\alpha_s(M_Z)$. In the following, this dependence is referred to as the *implicit dependence* of PDFs on $\alpha_s(M_Z)$.

For this reason, the value of $\alpha_s(M_Z)$ is provided for each PDF set in addition to the PDF parameters. Furthermore, global PDF fitting groups typically provide an entire series of PDFs fitted for a number of discrete values of $\alpha_s(M_Z)$. These PDF α_s series may be used to account for the implicit $\alpha_s(M_Z)$ dependence of the PDFs in additional studies.

This is of particular importance for $\alpha_s(M_Z)$ determinations from jet cross section measurements, as the corresponding theory calculations require PDFs as an input. Consequently, both the theoretical dependence of the cross section on $\alpha_s(M_Z)$ and the implicit dependence of the PDFs on $\alpha_s(M_Z)$ must be taken into account.

In the least-squares approach (section 3.2), the theory predictions are evaluated sequentially at multiple values of $\alpha_s(M_Z)$, until the minimum of the χ^2 quantity is found. In addition, theory predictions also depend on the PDF set, meaning that there is an additional, implicit dependence on the value of $\alpha_s(M_Z)$ associated with the PDF, which

is not *a priori* required to coincide with the value of $\alpha_s(M_Z)$ at which the theory is being evaluated. In order to maintain a clear notational distinction between these two quantities, they are denoted $\alpha_s(M_Z)_{\mathrm{PDF}}$ and $\alpha_s(M_Z)_{\mathrm{eval}}$, respectively.

It is worth noting here that the *implicit* dependence of the theory on $\alpha_s(M_Z)_{\mathrm{PDF}}$ is a side-effect of the PDF fitting procedure. In addition, due to $\alpha_s(M_Z)$ and the PDF parameters typically exhibiting a high degree of correlation in these fits, there is no guarantee that the dependence of PDFs on $\alpha_s(M_Z)$, as observed in these fits, can be directly identified with the theoretical QCD dependence, as postulated in the DGLAP evolution equations (2.13), since additional effects stemming from the PDF fitting procedure may also contribute. As a result, careful consideration of the theoretical implications is necessary when using the PDFs in an α_s series for determinations of $\alpha_s(M_Z)$.

A further aspect worth noting is the fact that PDFs are only available for several discrete values of $\alpha_s(M_Z)$. This poses a challenge for least-squares determinations of $\alpha_s(M_Z)$, since a fundamental requirement in this case is for the χ^2 quantity to be a continuous function of the fit parameters.

These issues are approached in $\alpha_s(M_Z)$ determinations by the H1, DØ and CMS collaborations in different ways.

Discussion of the H1, DØ and CMS Approaches

Each of the past determinations of $\alpha_s(M_Z)$ outlined in chapter 4 handles the issues outlined above in different ways. The H1 method does not account for the cross section dependence on $\alpha_s(M_Z)_{\mathrm{PDF}}$ during the χ^2 minimization. Instead, all fits are performed with PDFs for which the value of $\alpha_s(M_Z)$ has been fixed at 0.118. The implicit dependence on $\alpha_s(M_Z)_{\mathrm{PDF}}$ is assumed to introduce an additional uncertainty on the final value for $\alpha_s(M_Z)$, which is estimated by repeating the minimization using neighboring PDFs in the α_s series (section 4.1.1). This is referred to in the following as the "fixed PDF" method.

In contrast, the DØ collaboration chooses an interpolation-based method. In this approach, cross section predictions are calculated for each observable bin using all PDFs in an α_s series. Thus, a discrete set of cross section points is obtained, for which $\alpha_s(M_Z)_{\mathrm{eval}}$ is set to be equal to $\alpha_s(M_Z)_{\mathrm{PDF}}$. A continuous function for the cross section in each bin is obtained by interpolating these values using cubic splines. This is referred to as the "PDF interpolation" method.

Finally, in the CMS approach, rather than interpolating on the cross section level, the χ^2 quantity is evaluated for all values of $\alpha_s(M_Z)_{\mathrm{PDF}}$. The resulting points are shown to lie approximately on a parabola by performing a second-degree polynomial fit. The resulting curve is identified as a good approximation of the χ^2 near the minimum, allowing a best estimate and uncertainties for $\alpha_s(M_Z)$ to be extracted. In the following, this is referred to as the "χ^2 fit" method.

Each of the methods mentioned above have specific advantages and disadvantages. In the "fixed PDF" method, the choice of a particular value of $\alpha_s(M_Z)$ may introduce a bias on the resulting estimate for $\alpha_s(M_Z)$ towards this value. This bias is covered by

the additional "PDF α_s" uncertainty, which, however, needs to be estimated using additional techniques.

The "PDF interpolation" approach has the advantage of including the implicit cross section dependence on $\alpha_s(M_Z)_{\mathrm{PDF}}$ in the cross section predictions. A drawback of this method is the assumption that the implicit cross section dependence on $\alpha_s(M_Z)_{\mathrm{PDF}}$ is a good approximation of the theoretical cross section dependence on $\alpha_s(M_Z)$, as described by perturbation theory and the DGLAP evolution equations (2.13). However, this is not necessarily the case, since additional effects introduced via the PDF fitting procedure are not considered.

In addition, the "PDF interpolation" method has limited applicability in conjunction with PDF sets derived using Monte Carlo techniques, such as NNPDF. For these, each PDF in the α_s series is obtained by averaging over an ensemble of replicas. Since the number of replicas per ensemble is finite, the PDFs are subject to a natural statistical variation, which is also reflected in the theory predictions. An interpolation would treat these fluctuations as physically meaningful, causing predictions to become unreliable.

In the "χ^2 fit" method, no interpolation is done. Instead, the χ^2 quantity is calculated for each value of $\alpha_s(M_Z)_{\mathrm{PDF}}$, and a parabola is fitted to the resulting points. The main benefit of this method consists in avoiding some of the issues which arise due to interpolation: since $\alpha_s(M_Z)_{\mathrm{PDF}}$ is constant for every point, systematic effects stemming from the PDF fit procedure no longer determine the cross section dependence on $\alpha_s(M_Z)$, which instead results directly from the NLO calculation.

A significant disadvantage, however, are the limited possibilities of examining the uncertainties. One limitation concerns possible asymmetries exhibited by the discrete χ^2 points. Since the uncertainty of the $\alpha_s(M_Z)$ estimate is calculated from the necessarily parabolic χ^2 function resulting from the fit (see section 3.3), it is symmetric by construction. Thus, these asymmetries, if present, are not reflected in the uncertainty estimates.

Furthermore, the chosen χ^2 definition does not treat the fully correlated systematic uncertainties by means of nuisance parameters. For a detailed examination of these effects, a reformulation of the χ^2 quantity is required.

Another aspect is that, in this method, the final fit to the χ^2 points is performed without establishing an uncertainty model for the χ^2 values themselves. Thus, it is not possible to investigate the quality of this fit in terms of the deviations of individual χ^2 points from the fitted parabola. In particular situations, these deviations become large relative to the mean χ^2 value. This is observed in the case of NNPDF, due to the statistical variations outlined above, which are also reflected in the χ^2. In the absence of an appropriate uncertainty model for the χ^2 quantity, these variations lower the fit quality substantially and may be responsible for a bias of the final estimate for $\alpha_s(M_Z)$ and its uncertainties.

In light of the issues discussed above, the possibilities of performing a detailed study of uncertainties are found to be limited in the "χ^2 fit" method, in comparison to the other two methods, which rely on the iterative minimization of the χ^2 quantity. Consequently, the "χ^2 fit" approach is not explored further for the purpose of defining a unified fitting procedure.

In order to elucidate the implications of choosing either of the remaining two methods

for handling the implicit $\alpha_s(M_Z)$ dependence of the PDFs, a comparison study of the cross section dependence on $\alpha_s(M_Z)$ is performed. This is outlined in the following section.

Cross Section Dependence on $\alpha_s(M_Z)$

In the preceding section, the "fixed PDF" and "PDF interpolation" methods of accounting for the implicit dependence of PDFs on $\alpha_s(M_Z)$ are presented. The latter approach is based on the assumption that the cross section as a function of $\alpha_s(M_Z)_{\mathrm{PDF}}$, as calculated for discrete $\alpha_s(M_Z)$ points using the PDFs in an α_s series, is a good approximation of the theoretical cross section dependence on $\alpha_s(M_Z)$, as described by the theory.

As a rough indicator of the quality of this approximation, a comparison of the cross section predictions computed with the "fixed PDF" and "PDF interpolation" methods is performed. Since the dominant, leading-order contribution to the cross section for inclusive jet production in hadron-hadron collisions is quadratic in $\alpha_s(M_Z)$, this dependence is expected to be seen for the corresponding theory predictions for both methods.

In figure 6.2, the two methods are compared. Shown are the double-differential inclusive jet cross section predictions for the CMS dataset for two observable bins and several PDF sets. Whereas the curves for the "fixed PDF" method follow the expected theoretical dependence of inclusive jet cross sections on $\alpha_s(M_Z)$, the "PDF interpolation" method yields a different dependence. An expanded set of such plots, showing this dependence for four data points of the CMS dataset situated in four different kinematic regions, is available in appendix A.

This effect is particularly striking at high transverse momenta and outer rapidities, where the uncertainties become large and data available for constraining the PDFs are scarce. For instance, predictions obtained with the MSTW2008 PDF set for the observable bin with transverse momenta ranging from 638 to 686 GeV and absolute rapidities between 2 and 2.5 show a near-insensitivity to the PDF $\alpha_s(M_Z)$, even showing a slight downwards trend at low values of $\alpha_s(M_Z)$. This is most probably caused by the limited constraining power of the data in this phase space region. In particular, since the gluon PDF at low x cannot be constrained sufficiently by the jet measurements included in the MSTW2008 PDF determination, this correlation remains high, potentially leading to a nearly full compensation of $\alpha_s(M_Z)$ by the PDF gluon parameters.

Overall, however, the most significant differences between the "fixed PDF" and "PDF interpolation" methods occur for kinematic regions where experimental and theoretical uncertainties are relatively large. Consequently, the choice of method is not expected to have a large impact on the fit results.

For the unified fitting procedure, the implicit $\alpha_s(M_Z)$ dependence of PDFs is accounted for via the "fixed PDF" approach. Alternate estimations are also performed using the "PDF interpolation" method and compared to the "fixed PDF" method. The resulting estimates of $\alpha_s(M_Z)$ do not show significant differences between the two methods. An overview of results obtained with the alternative method is given in appendix B.

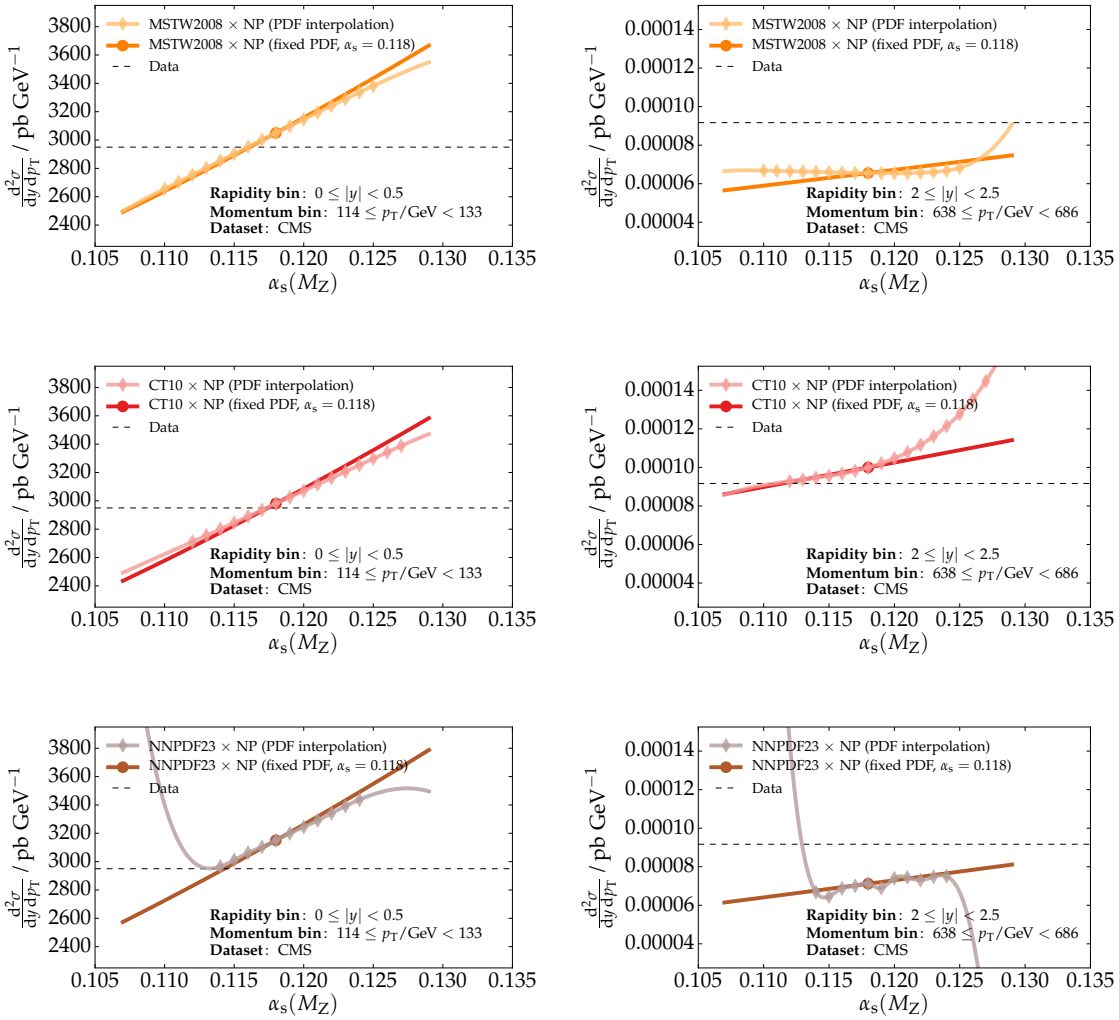

Figure 6.2.: Comparison of the CMS inclusive jet cross section dependence on $\alpha_s(M_Z)$ for the "fixed PDF" and "PDF interpolation" methods, shown here for the MSTW2008, CT10 and NNPDF2.3 PDF sets (all NLO). In the "fixed PDF" method, cross sections are calculated using the PDF of the α_s series with $\alpha_s(M_Z) = 0.118$. In the "PDF Interpolation" method, cross sections are calculated by interpolating between the predictions obtained with each PDF of the α_s series using cubic splines. Whereas at low p_T and central rapidities *(left column)*, only a slight difference can be observed, the effect is much more pronounced at high p_T and outer rapidities *(right column)*. The statistical variation inherent to NNPDF *(bottom row)* causes significant deviations between the methods, particularly in the extrapolation region.

6.2.2. Uncertainty Model and Definition of a χ^2 Quantity

A next step towards a unified fitting procedure consists in establishing a model for experimental and theoretical uncertainties. On the basis of this model, a χ^2 quantity measuring the level of agreement between the data and the theory predictions may be defined in terms of the theory parameters. In this section, a number of theoretical and practical aspects regarding the choice of an uncertainty model are discussed, and a χ^2 definition for the unified fitting procedure is chosen.

For all datasets, the uncertainties on the cross section measurements are dominated by systematic effects, which are predominantly multiplicative in nature. Accordingly, the measurements are modeled as stochastic variables drawn from a log-normal probability distribution. This is equivalent to modeling the logarithms of the measurements as being drawn from a Gaussian distribution, allowing the least-squares approach described in chapter 3.2 to be used.

Furthermore, since the log-normal distribution converges towards a Gaussian distribution for small variances, additive effects of sufficiently small magnitude may be treated as multiplicative without introducing a significant bias. For this reason, Poisson uncertainties on measurements due to statistical fluctuations, which are mostly small compared to the systematic uncertainties, are also described reasonably well in this manner. Conversely, a fully additive treatment of multiplicative systematics would result in a larger bias.

A number of systematic effects contributing to the uncertainty on the theory may also be treated as multiplicative. This applies, for instance, to the uncertainty due to non-perturbative correction factors, which are multiplicative by construction. Furthermore, the uncertainties on the PDFs, as provided by the PDF fitting group, are also taken as multiplicative

This is justified since PDFs or linear combinations thereof appear as multiplicative factors in the theoretical expressions describing inclusive jet cross sections (2.12), (2.14), as well as in the fast interpolation performed with fastNLO (5.5).

The remaining systematic effects consist primarily of procedural uncertainties arising from the necessity to choose from a particular set of available PDF sets or PDFs fitted at different values of $\alpha_s(M_Z)$. Since no meaningful assumption can be made regarding the probability distribution of these effects, they are not included in the χ^2 definition, but are estimated using additional techniques. The same is true for uncertainties due to missing higher orders in the perturbative calculation. As described in section 3.3, these can be estimated by performing the fit at additional values of the renormalization and factorization scales. The resulting uncertainty estimate on $\alpha_s(M_Z)$ is referred to as the "scale" uncertainty.

In light of the above points, the χ^2 quantity for the unified estimation procedure may thus be defined as:

$$\chi^2_{\text{Unif}} = \mathbf{p}^\top \left(\mathbf{V}^{(\text{exp})}_{\text{rel}} + \mathbf{V}^{(\text{PDF})}_{\text{rel}} + \mathbf{V}^{(\text{NP})}_{\text{rel}} \right)^{-1} \mathbf{p} \tag{6.1}$$

The residuals $\mathbf{p}$ are defined as:

$$p_i = \ln \frac{m_i}{t_i} \tag{6.2}$$

The above definition is analogous to that used by the H1 collaboration (section 4.1.1). In contrast to the H1 definition, however, the covariance matrices for PDF and non-perturbative (NP) uncertainties are included in the definition.

For the actual estimation procedure, an equivalent formulation of the above expression in terms of nuisance parameters is used. This is constructed analogously to (4.2), (4.3), and (4.4), with one nuisance parameter being introduced to account for each fully correlated systematic effect. In particular, PDF uncertainties obtained via the "Hessian" method from LHAPDF 6 are assumed to be fully correlated for each eigenvector variation, thus introducing one nuisance parameter per eigenvector.

A significant advantage of this χ^2 quantity is the use of the covariance matrix calculated from relative uncertainties. Since these do not change for multiplicative uncertainties, the total covariance matrix only needs to be calculated and inverted once before the fit procedure. Furthermore, any nonlinearities introduced by parameter-dependent covariance matrices are avoided.

6.2.3. Extraction of $\alpha_s(M_Z)$ and Uncertainty Estimation

A final aspect of the unified fitting procedure is the extraction of $\alpha_s(M_Z)$ and the estimation of uncertainties. A best estimate for $\alpha_s(M_Z)$ is obtained in the least-squares approach by iteratively minimizing the χ^2 quantity (6.1) with respect to $\alpha_s(M_Z)$.

Primarily, the estimation of uncertainties on this estimate is performed by performing a profile scan of the χ^2 near the minimum, as described in section 3.3. The one-sigma confidence interval on $\alpha_s(M_Z)$ corresponding to a unit increase in χ^2 is quoted as the uncertainty.

Since the χ^2 definition includes experimental, non-perturbative, and Hessian PDF uncertainties, the uncertainty on $\alpha_s(M_Z)$ extracted in this way is further broken down into its individual contributions by successively removing the covariance matrices for the PDF and non-perturbative uncertainties, and repeating the minimization and error estimation. The uncertainty for each individual effect is obtained by subtracting (in quadrature) the uncertainty estimates obtained with and without the respective contributions to the total covariance matrix. Experimental uncertainties are estimated by including only the experimental covariance matrix in the χ^2 definition.

In addition to the uncertainties included in the χ^2 definition, two additional procedural uncertainties are estimated, in order to remain conservative. Since these are not derived from the behavior of the χ^2 quantity at the minimum, they cannot be interpreted as confidence intervals, but give only an approximate indication of the magnitude of the associated effects.

First, due to the availability of multiple global PDF sets with different methods used for their determination, the final estimate of $\alpha_s(M_Z)$ is expected to show a degree of variation depending on which PDF set is used. In order to account for this, a *PDF set*

uncertainty is estimated by performing the determination with several different PDF sets.

Calculations for the ABM11 and HERAPDF2.0 PDF sets do not describe the data as well as the other PDF sets examined, confirming the observations made in past determinations of $\alpha_s(M_Z)$ (see section 4.1). Thus, estimates of $\alpha_s(M_Z)$ derived from these PDF sets are not considered in the estimation of this uncertainty. Estimations of $\alpha_s(M_Z)$ are performed with the MSTW2008, MMHT2014, CT10 and CT14 PDF sets, taking the maximal variations away from the central estimate for $\alpha_s(M_Z)$ to represent an additional, asymmetric *PDF set* uncertainty. The central value is quoted for the MMHT2014 PDF set.

In the "fixed PDF" method, the necessity of choosing one PDF from those available in an α_s series arises. For the central estimate of $\alpha_s(M_Z)$, the PDF set with $\alpha_s(M_Z) = 0.118$ is chosen. In order to account for the possible bias resulting from this choice, an associated uncertainty is estimated by repeating the determination using PDFs with a value for $\alpha_s(M_Z)$ of 0.116 and 0.120 for the "down" and "up" variations, respectively. The resulting variations with respect to the central value are quoted as an additional, asymmetric *PDF* α_s uncertainty. For PDF α_s series lacking these values, the PDFs corresponding to the next largest available variation away from $\alpha_s(M_Z) = 0.118$ are used.

6.3. Fit to the Individual Datasets Using the Unified Fit Procedure

The unified fitting procedure described above can now be applied separately to the individual datasets. In order to gauge the impact of the fitting procedure itself on the resulting estimates, these are compared to the original publication results.

A comparison of the results obtained with the fitting methods used in the original publications and the unified fitting procedure is presented in table 6.2. In terms of the central estimates of $\alpha_s(M_Z)$ and the experimental uncertainties, a good general agreement between the two methods can be seen for all datasets, with all observed changes in the central estimate being covered by the experimental uncertainty. For the DØ NLO fit, only a total uncertainty is published, which covers both experimental and theoretical uncertainties. Thus, a direct comparison of experimental uncertainties is not possible in this case.

Due to the changes in fitting methodology, such as the use of a different error model for measurements and theory predictions, small overall differences between the values obtained with the unified fitting procedure and the publication values are expected. This is consistent with the observed values, with the estimates for the H1 dataset being more similar for both methods, whereas the DØ and CMS results show larger differences.

In order to ascertain the fit quality, the value of the χ^2 quantity at the minimum is compared to the number of degrees of freedom. As shown in table 6.2, this figure is close to unity for all fits, indicating a good fit quality.

In conclusion, the unified fitting procedure is found to be applicable for a determination of $\alpha_s(M_Z)$ from each of the individual datasets, producing results which are com-

		Central value $\alpha_s(M_Z)$	Experimental uncertainty	PDF set (NLO)
H1	Publication	0.1174	$\pm$0.0022	MSTW2008
	Unified Procedure	0.1170	$\pm$0.0022	
	$\hookrightarrow \chi^2/\text{ndf} \approx 24/23 = 1.04$			
DØ (NLO)	Publication	0.1203	*(breakdown not published)*	MSTW2008
	Unified Procedure	0.1238	$\pm$0.0050	
	$\hookrightarrow \chi^2/\text{ndf} \approx 17/21 = 0.81$			
CMS	Publication	0.1185	$\pm$0.0019	CT10
	Unified Procedure	0.1177	$\pm$0.0023	
	$\hookrightarrow \chi^2/\text{ndf} \approx 107/132 = 0.81$			

Table 6.2.: Comparison of results obtained with the unified fitting procedure and the original publication results. Shown are estimates for $\alpha_s(M_Z)$ and the experimental uncertainty extracted from each of the three datasets. In obtaining the results using the unified procedure the same PDF set used by the original publications for their main estimate is used. A good agreement can be seen between the original quotes and the results obtained using the unified procedure, with all observed differences being covered by the experimental uncertainties. Also shown are the reduced χ^2 values for fits performed with the unified procedure, all of which are close to unity, indicating a good fit quality.

patible with past $\alpha_s(M_Z)$ determinations. Consequently, all three datasets may be used simultaneously in conjunction with the unified fitting procedure in order to obtain a more precise estimate for $\alpha_s(M_Z)$.

6.4. Fit to the Combined Datasets

One important issue when more than one dataset is included in a parameter estimation procedure is identifying and establishing the degree of correlation between the individual measurements and between the theory predictions calculated for each dataset.

In this approach, since the measurements have been conducted by experiments at three different colliders, no correlations are assumed to exist between the experimental measurements across datasets.

In contrast, theory predictions require a more differentiated treatment. For instance, since the calculation of non-perturbative corrections is specialized to each of the individual experiments, and different methods of estimating the corresponding uncertainties are used by the collaborations, it is reasonable to assume these to be largely uncorrelated across datasets. Thus, the nuisance parameters introduced to account for non-perturbative effects only relate to the individual datasets.

For Hessian PDF uncertainties, however, this is not the case, as the nuisance param-

eters introduced per PDF eigenvector variation simultaneously affect all cross section predictions across the datasets. Thus, each of the Hessian PDF uncertainties associated with the PDF eigenvector variations is taken to be fully correlated across datasets and is assigned a nuisance parameter.

In estimating the procedural PDF and scale uncertainties, the variation of the central estimate resulting from a variation of the underlying effect is considered. These uncertainties are therefore correlated between the datasets by construction.

After establishing the correlation model for the datasets, the extraction of $\alpha_s(M_Z)$ can be performed for the combined datasets. An overview of the resulting estimates for $\alpha_s(M_Z)$ and the different uncertainty contributions can be seen in table 6.3 and figure 6.3, along with the extractions from the individual datasets. The final estimate for $\alpha_s(M_Z)$ obtained is:

$$\begin{aligned}\alpha_s(M_Z) = 0.1172 \; &^{+0.0015}_{-0.0015}\,(\text{exp}) \; ^{+0.0009}_{-0.0009}\,(\text{PDF, MMHT}) \; ^{+0.0005}_{-0.0005}\,(\text{NP}) \\ &^{+0.0011}_{-0.0004}\,(\text{PDF set}) \; ^{+0.0007}_{-0.0003}\,(\text{PDF } \alpha_s) \; ^{+0.0057}_{-0.0042}\,(\text{scale})\end{aligned} \tag{6.3}$$

	Central value	**Uncertainties** (scaled by a factor of 10^3)					
	$\alpha_s(M_Z)$	(exp)	(PDF)	(NP)	(PDF set)	(PDF α_s)	(scale)
H1	0.1168	$^{+2.2}_{-2.2}$	$^{+0.7}_{-0.7}$	$^{+0.9}_{-0.9}$	$^{+0.3}_{-0.0}$	$^{+1.0}_{-0.4}$	$^{+5.9}_{-4.7}$
↪ $\chi^2/\text{ndf} \approx 23/23 = 1.00$							
DØ (NLO)	0.1240	$^{+5.1}_{-4.9}$	$^{+1.9}_{-1.8}$	$^{+3.3}_{-3.1}$	$^{+1.0}_{-0.3}$	$^{+0.0}_{-0.4}$	$^{+9.7}_{-4.8}$
↪ $\chi^2/\text{ndf} \approx 17/21 = 0.81$							
CMS	0.1154	$^{+2.2}_{-2.1}$	$^{+1.9}_{-1.8}$	$^{+0.1}_{-0.1}$	$^{+2.3}_{-0.8}$	$^{+0.5}_{-0.2}$	$^{+5.9}_{-3.1}$
↪ $\chi^2/\text{ndf} \approx 110/132 = 0.83$							
[H1, DØ, CMS]	0.1172	$^{+1.5}_{-1.5}$	$^{+0.9}_{-0.9}$	$^{+0.5}_{-0.5}$	$^{+1.1}_{-0.4}$	$^{+0.7}_{-0.3}$	$^{+5.7}_{-4.2}$
↪ $\chi^2/\text{ndf} \approx 152/178 = 0.85$							

Table 6.3.: Results obtained with the unified fitting procedure from fits to each individual dataset and to the combined datasets. Shown are the central estimates for $\alpha_s(M_Z)$, as well as the individual contributions to the total uncertainty, obtained for the MMHT2014 PDF set (NLO) using the "fixed PDF" method.

The results obtained for the combined datasets are compatible with the results of the individual fits. The uncertainties extracted from the behavior of the χ^2 quantity in the minimum (experimental, PDF and non-perturbative uncertainties) are approximately symmetric in all cases. Thus, no significant indication for a potential inadequacy of the chosen uncertainty models for the measurements and the theory predictions is observed. The remaining uncertainties are asymmetric by construction.

Overall, the extraction of $\alpha_s(M_Z)$ from the combined datasets exhibits a reduced experimental uncertainty with respect to each of the individual fits. Furthermore, some reduction of the Hessian PDF and non-perturbative uncertainties is also observed. The largest uncertainty contribution by far remains the scale uncertainty, which reaches ap-

proximately 5% of the central value. This uncertainty is expected to be reduced for extractions performed with theory predictions calculated at next-to-next-to-leading order accuracy, which have recently become available [41].

6.5. Conclusion

In this chapter, the development and evaluation of techniques for the determination of $\alpha_s(M_Z)$ from multiple sets of inclusive jet measurements have been presented. These techniques have been implemented in the Alpos package at next-to-leading order accuracy and the obtained results have been evaluated.

After successfully reproducing results from past determinations of $\alpha_s(M_Z)$ with the Alpos framework, a unified procedure for the extraction of a best estimate for $\alpha_s(M_Z)$ and the detailed estimation of uncertainties has been developed under consideration of several theoretical and technical aspects.

An application of this procedure to the individual datasets yields results which are compatible with those obtained from past determinations and show a good level of agreement among themselves and with the world average value of $\alpha_s(M_Z)$.

Applying these techniques in a determination using all datasets simultaneously yields an estimate of $\alpha_s(M_Z)$ with a reduced experimental uncertainty. The largest uncertainty contribution, however, stems from missing higher orders in perturbation theory. A further improvement in the determination accuracy is expected for next-to-next-to-leading order accuracy.

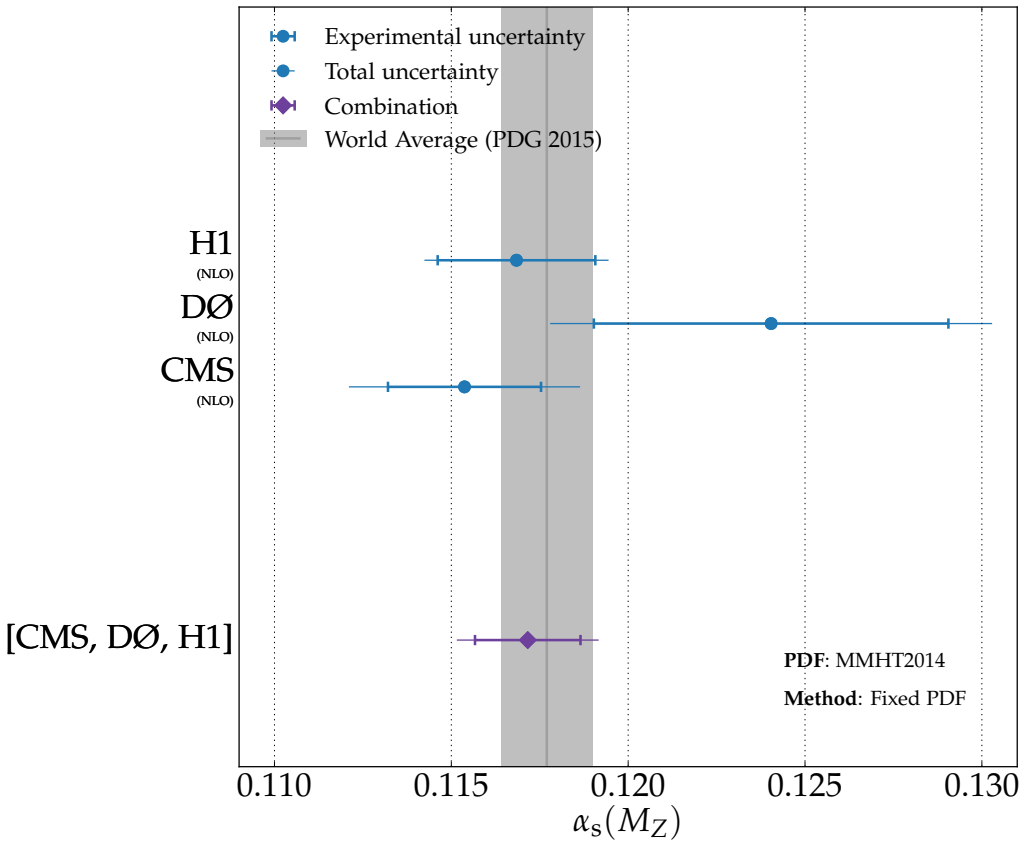

Figure 6.3.: Extractions of $\alpha_s(M_Z)$ from the individual and combined datasets using the unified fitting procedure. Shown are the central results obtained for $\alpha_s(M_Z)$, as well as the experimental and total uncertainties. To avoid overshadowing the other uncertainties, the dominant scale uncertainty is not included in the total uncertainty shown. The value of $\alpha_s(M_Z)$ is in good agreement with the individual estimates and the world average.

7. Summary and Outlook

In this thesis, a method for the determination of the strong coupling constant $\alpha_s(M_Z)$ from measurements of inclusive jet production cross sections performed at multiple experiments has been developed. To this end, $\alpha_s(M_Z)$ extractions from inclusive jet cross section measurements at the H1, DØ, and CMS experiments, as performed by the respective collaborations, have been analyzed and compared in terms of experimental and theoretical considerations, as well as the results obtained for $\alpha_s(M_Z)$.

The original procedures, as well as the procedure established in this work, have been implemented in the Alpos framework, a recently developed public software package for data-to-theory comparisons and parameter estimation, to which significant contributions have been made as part of this thesis. The originally published estimates for $\alpha_s(M_Z)$ are reproduced within this framework.

Estimates for $\alpha_s(M_Z)$ are then obtained with the developed extraction procedure, both for the individual datasets and for the combined dataset.s The results are found to be in agreement with the originally published estimates, as well as with each other and with the current world average value for $\alpha_s(M_Z)$. In addition, a reduction of the experimental uncertainty is observed for the combined extraction, which yields the following result for the strong coupling constant:

$$\begin{aligned}\alpha_s(M_Z) = 0.1172 \; &^{+0.0015}_{-0.0015}\,(\text{exp}) \; ^{+0.0009}_{-0.0009}\,(\text{PDF, MMHT}) \; ^{+0.0005}_{-0.0005}\,(\text{NP}) \\ &^{+0.0011}_{-0.0004}\,(\text{PDF set}) \; ^{+0.0007}_{-0.0003}\,(\text{PDF } \alpha_s) \; ^{+0.0057}_{-0.0042}\,(\text{scale})\end{aligned}$$

The uncertainty due to missing higher orders in perturbative calculations remains the dominant contribution to the total uncertainty at approximately 5% of the reference value.

The focus of this work consists in performing a simultaneous determination of the strong coupling constant from a number of well-documented measurements of inclusive jet production cross sections, for which associated extractions of $\alpha_s(M_Z)$ were available.

Several possibilities for further expanding the scope of this analysis can be identified. One means of achieving this consists in making use of a larger phase space than the original determinations by revising the exclusion criteria for individual data points. Similarly, an advantage can be gained from incorporating measurements of jet cross section ratios or, in the case of ep scattering, jet observables normalized to neutral current DIS cross sections. As both types of measurements benefit from a reduced systematic uncertainty, this will be reflected in the final estimate for $\alpha_s(M_Z)$.

Furthermore, in light of the availability of further measurements concerning jet observables from multiple experimental collaborations, these can also be included in a combined determination. An additional aspect to consider here are the experimental

correlations between experiments at the same accelerator facility.

A further aspect concerns the determination of non-perturbative corrections to the theory calculations. Deriving these and the corresponding uncertainties in a consistent manner represents a further step toward a fully harmonized combined determination procedure.

In addition, a central point in the $\alpha_s(M_Z)$ determination procedure concerns the implicit dependence of PDFs on the value of $\alpha_s(M_Z)$ assumed for their determination. The need for taking this into account can be eliminated by performing a simultaneous determination of $\alpha_s(M_Z)$ and the PDFs.

Last, but not least, the combined determination of $\alpha_s(M_Z)$ in this work has been carried out using perturbative QCD calculations performed at next-to-leading order accuracy. As next-to-next-to-leading order calculations become available, the accuracy of the $\alpha_s(M_Z)$ determination can be further improved.

Appendix A. Dependence of Inclusive Jet Cross Sections on $\alpha_s(M_Z)$

In chapter 6, two methods of accounting for the implicit dependence of PDFs on $\alpha_s(M_Z)$ are described: the "fixed PDF" and "PDF interpolation" methods. Each method leads to a different dependence of the cross section predictions on $\alpha_s(M_Z)$.

In the following, this difference is illustrated for predictions obtained with different PDF sets using a selection of four phase space points from the CMS dataset.

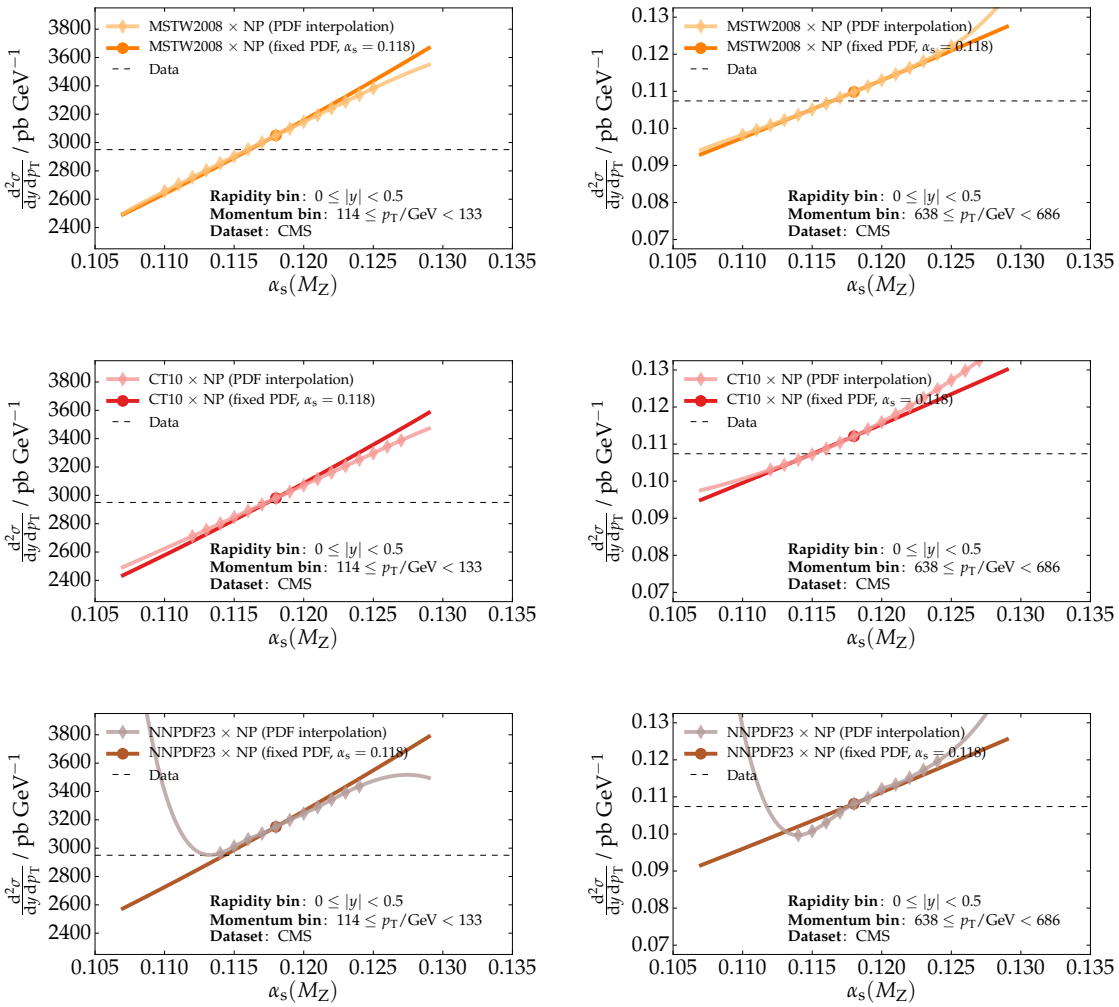

Figure A.1.: Dependence of the differential inclusive jet cross section for the CMS dataset at central rapidities. Shown above are the dependences calculated for the MSTW2008, CT10 and NNPDF2.3 (NLO) PDF sets at low p_T *(left column)* and medium p_T *(right column)*.

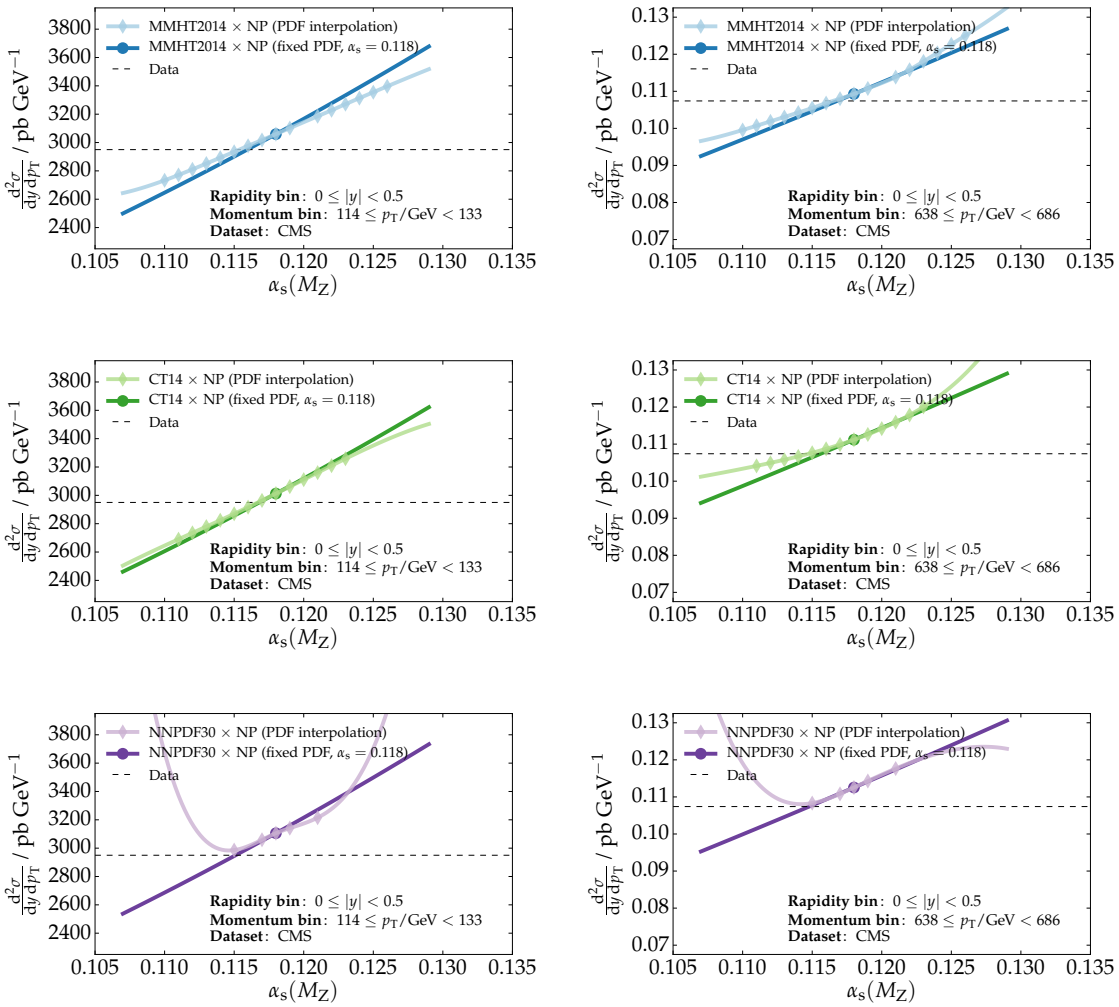

Figure A.2.: Dependence of the differential inclusive jet cross section for the CMS dataset at central rapidities. Shown above are the dependences calculated for the MMHT2014, CT14 and NNPDF3.0 (NLO) PDF sets at low p_T *(left column)* and medium p_T *(right column)*.

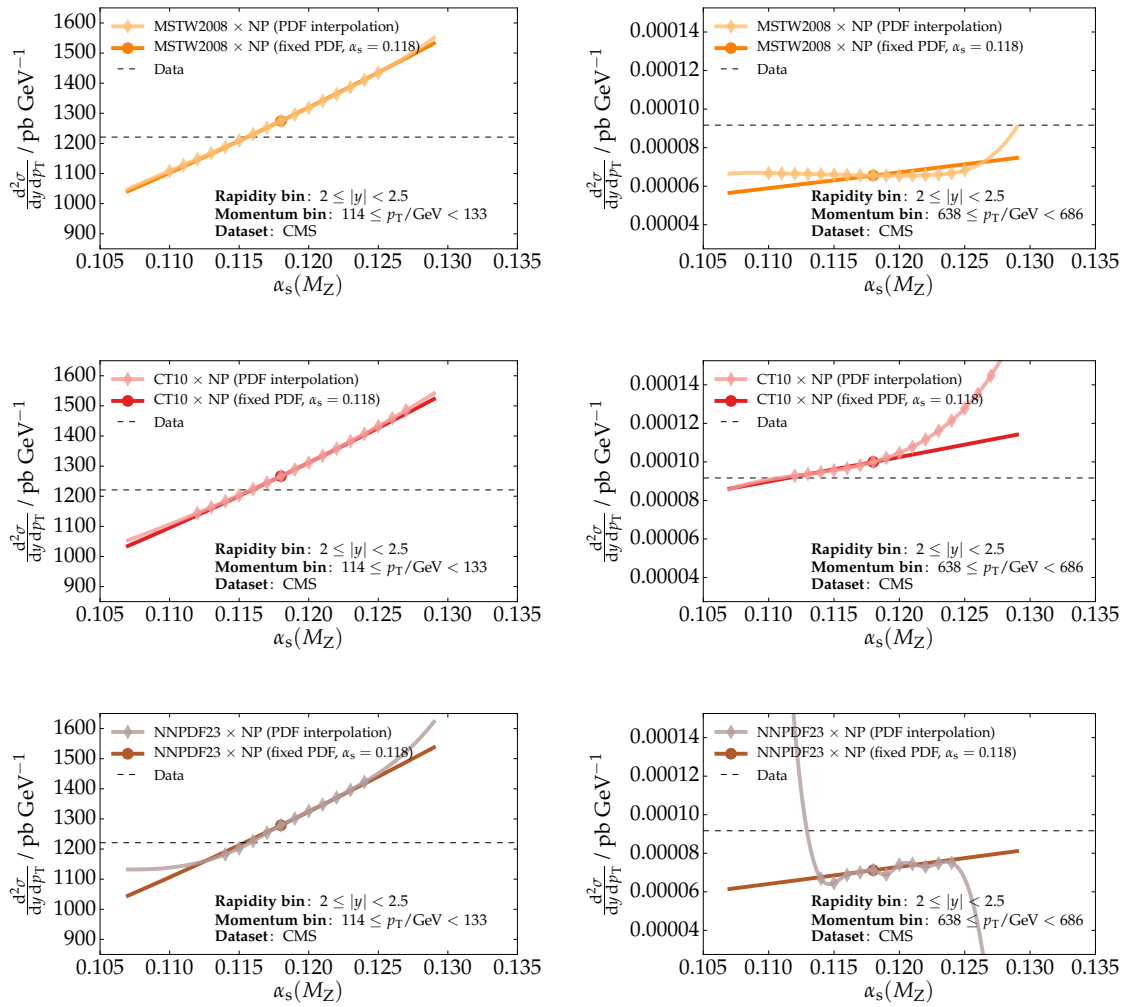

Figure A.3.: Dependence of the differential inclusive jet cross section for the CMS dataset at outer rapidities. Shown above are the dependences calculated for the MSTW2008, CT10 and NNPDF2.3 (NLO) PDF sets at low p_T *(left column)* and medium p_T *(right column)*.

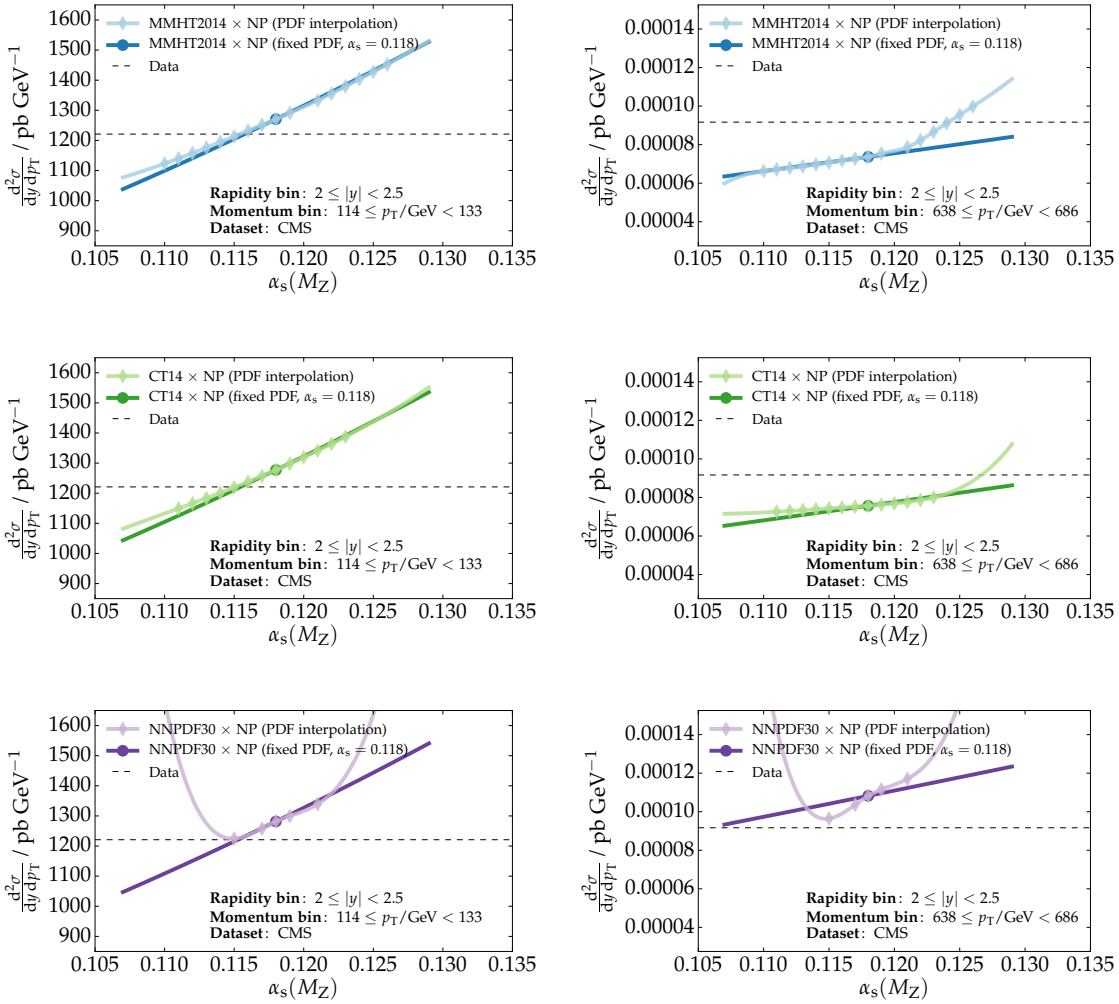

Figure A.4.: Dependence of the differential inclusive jet cross section for the CMS dataset at outer rapidities. Shown above are the dependences calculated for the MMHT2014, CT14 and NNPDF3.0 (NLO) PDF sets at low p_T *(left column)* and medium p_T *(right column)*.

Appendix B. Results with the "PDF Interpolation" Method

In performing the extraction of $\alpha_s(M_Z)$ in chapter 6, two methods of accounting for the implicit dependence of PDFs on $\alpha_s(M_Z)$ are explored. As a result of theoretical considerations (see section 6.2.1), the "fixed PDF" method is chosen as the main method for obtaining estimates for $\alpha_s(M_Z)$ in this analysis. Alternate estimates, which have been obtained using the "PDF interpolation" method, are provided in table B.1.

	Central value $\alpha_s(M_Z)$	**Uncertainties** (scaled by a factor of 10^3) (exp)	(PDF)	(NP)	(PDF set)	(scale)
H1	0.1167	$^{+2.8}_{-2.6}$	$^{+0.5}_{-0.6}$	$^{+0.9}_{-0.7}$	$^{+0.6}_{-0.1}$	$^{+4.7}_{-4.9}$
↪ $\chi^2/\text{ndf} \approx 23/23 = 1.00$						
DØ (NLO)	0.1214	$^{+3.9}_{-4.7}$	$^{+1.6}_{-1.6}$	$^{}_{-}{}^{\dagger}$	$^{+1.1\,\ddagger}_{-0.0}$	$^{+6.0}_{-3.6}$
↪ $\chi^2/\text{ndf} \approx 17/21 = 0.81$						
CMS	0.1144	$^{+2.3}_{-2.3}$	$^{+2.1}_{-2.0}$	$^{}_{-}{}^{\dagger}$	$^{+3.5\,\ddagger}_{-0.0}$	$^{+9.5}_{-2.9}$
↪ $\chi^2/\text{ndf} \approx 109/132 = 0.83$						
[H1, DØ, CMS]	0.1167	$^{+1.5}_{-1.8}$	$^{+1.5}_{-0.6}$	$^{+0.3}_{-0.4}$	$^{+1.7}_{-0.3}$	$^{+7.3}_{-4.5}$
↪ $\chi^2/\text{ndf} \approx 152/178 = 0.85$						

Table B.1.: Results obtained with the unified fitting procedure from fits to each individual dataset and to the combined datasets using the "PDF interpolation" method. Shown are the central estimates for $\alpha_s(M_Z)$, as well as the individual contributions to the total uncertainty, obtained for the MMHT2014 PDF set (NLO). In a number of cases (†), individual uncertainties could not be estimated by subtraction in quadrature due to the overall uncertainty decreasing upon inclusion of these uncertainties in the χ^2 definition. The PDF set uncertainties are calculated as the maximal spread of the best estimates obtained with the MSTW2008, MMHT2014, CT10 and CT14 (NLO) PDF sets. This procedure leads to the estimation of these uncertainties as zero (‡) if the value of $\alpha_s(M_Z)$ obtained with the MMHT2014 PDF set is an extreme value.

Bibliography

[1] Y. L. Dokshitzer, "Calculation of the Structure Functions for Deep Inelastic Scattering and e+ e- Annihilation by Perturbation Theory in Quantum Chromodynamics.," *Sov. Phys. JETP* **46** (1977) 641.

[2] V. Gribov and L. Lipatov, "Deep inelastic ep scattering in perturbation theory," *Sov. J. Nucl. Phys.* **15** (1972) 438.

[3] G. Altarelli and G. Parisi, "Asymptotic Freedom in Parton Language," *Nucl. Phys. B* **126** (1977) 298. doi:10.1016/0550-3213(77)90384-4.

[4] L. Harland-Lang, A. Martin, P. Motylinski, and R. Thorne, "Parton distributions in the LHC era: MMHT 2014 PDFs," *Eur. Phys. J. C* **75** (2015), no. 5, 204, arXiv:1412.3989. doi:10.1140/epjc/s10052-015-3397-6.

[5] A. D. Martin, W. J. Stirling, R. S. Thorne, and G. Watt, "Parton distributions for the LHC," *Eur. Phys. J. C* **63** (2009) 189, arXiv:0901.0002. doi:10.1140/epjc/s10052-009-1072-5.

[6] J. Gao, M. Guzzi, J. Huston, H.-L. Lai, Z. Li, et al., "CT10 next-to-next-to-leading order global analysis of QCD," *Phys. Rev. D* **89** (2014), no. 3, 033009, arXiv:1302.6246. doi:10.1103/PhysRevD.89.033009.

[7] S. Dulat, T. J. Hou, J. Gao, M. Guzzi, J. Huston, et al., "The CT14 Global Analysis of Quantum Chromodynamics," arXiv:1506.07443.

[8] R. D. Ball et al., "Parton distributions with LHC data," *Nucl. Phys.* **B867** (2013) 244–289, arXiv:1207.1303. doi:10.1016/j.nuclphysb.2012.10.003.

[9] **NNPDF** Collaboration, R. D. Ball et al., "Parton distributions for the LHC Run II," *JHEP* **04** (2015) 040, arXiv:1410.8849. doi:10.1007/JHEP04(2015)040.

[10] **H1, ZEUS** Collaboration, H. Abramowicz et al., "Combination of Measurements of Inclusive Deep Inelastic $e^{\pm}p$ Scattering Cross Sections and QCD Analysis of HERA Data," arXiv:1506.06042.

[11] S. Alekhin, J. Blümlein, and S.-O. Moch, "ABM11 parton distributions and benchmarks," arXiv:1208.1444. doi:10.3204/DESY-PROC-2012-02/302.

[12] K. Olive et al. (Particle Data Group), "Review of Particle Physics," *Chin. Phys. C* **38** (2014) 090001. (2015 update). doi:10.1088/1674-1137/38/9/090001.

[13] S. Catani, Y. L. Dokshitzer, M. Olsson, G. Turnock, and B. R. Webber, "New clustering algorithm for multijet cross sections in e+ e- annihilation," *Phys. Lett. B* **269** (1991) 432. doi:10.1016/0370-2693(91)90196-W.

[14] M. Cacciari, G. P. Salam, and G. Soyez, "The anti-k_t jet clustering algorithm," *JHEP* **04** (2008) 063, arXiv:0802.1189. doi:10.1088/1126-6708/2008/04/063.

[15] G. C. Blazey et al. in *Proceedings of the Workshop: "QCD and Weak Boson Physics in Run II"*, p. 47. Batavia, Illinois, 2000. Fermilab-Pub-00/297, Section 3.5.

[16] A. Banfi, G. P. Salam, and G. Zanderighi, "Phenomenology of event shapes at hadron colliders," *JHEP* **06** (2010) 038, arXiv:1001.4082. doi:10.1007/JHEP06(2010)038.

[17] **H1** Collaboration, V. Andreev et al., "Measurement of multijet production in ep collisions at high Q^2 and determination of the strong coupling α_s," *Eur. Phys. J. C* **75** (2015) 65, arXiv:1406.4709. doi:10.1140/epjc/s10052-014-3223-6.

[18] K. Charchula, G. A. Schuler, and H. Spiesberger, "Combined QED and QCD radiative effects in deep inelastic lepton - proton scattering: The Monte Carlo generator DJANGO6," *Comput. Phys. Commun.* **81** (1994) 381. doi:10.1016/0010-4655(94)90086-8.

[19] H. Jung, "Hard diffractive scattering in high energy ep collisions and the Monte Carlo generator RAPGAP," *Computer Physics Communications* **86** (1995), no. 1, 147–161.

[20] G. Ingelman, A. Edin, and J. Rathsman, "LEPTO 6.5 - A Monte Carlo Generator for Deep Inelastic Lepton-Nucleon Scattering," *Comput. Phys. Commun.* **101** (1997) 108, arXiv:hep-ph/9605286. doi:10.1016/S0010-4655(96)00157-9.

[21] J. Pumplin, D. Stump, R. Brock, D. Casey, J. Huston, et al., "Uncertainties of predictions from parton distribution functions. 2. The Hessian method," *Phys. Rev. D* **65** (2001) 014013, arXiv:hep-ph/0101032. doi:10.1103/PhysRevD.65.014013.

[22] T. Gleisberg, S. Höche, F. Krauss, M. Schönherr, S. Schumann, et al., "Event generation with SHERPA 1.1," *JHEP* **02** (2009) 007, arXiv:0811.4622. doi:10.1088/1126-6708/2009/02/007.

[23] **D0** Collaboration, V. Abazov et al., "Measurement of the inclusive jet cross-section in $p\bar{p}$ collisions at $\sqrt{s} = 1.96$ TeV," *Phys. Rev. Lett.* **101** (2008) 062001, arXiv:0802.2400. doi:10.1103/PhysRevLett.101.062001.

[24] **D0** Collaboration, V. Abazov et al., "Determination of the strong coupling constant from the inclusive jet cross section in $p\bar{p}$ collisions at $\sqrt{s} = 1.96$ TeV," *Phys. Rev. D* **80** (2009) 111107, arXiv:0911.2710. doi:10.1103/PhysRevD.80.111107.

[25] A. D. Martin, R. G. Roberts, W. J. Stirling, and R. S. Thorne, "Physical gluons and high E(T) jets," *Phys. Lett.* **B604** (2004) 61–68, arXiv:hep-ph/0410230. doi:10.1016/j.physletb.2004.10.040.

[26] W. K. Tung et al., "Heavy quark mass effects in deep inelastic scattering and global QCD analysis," *JHEP* **02** (2007) 053, arXiv:hep-ph/0611254. doi:10.1088/1126-6708/2007/02/053.

[27] N. Kidonakis and J. F. Owens, "Effects of higher-order threshold corrections in high-E_T jet production," *Phys. Rev. D* **63** (Feb, 2001) 054019. doi:10.1103/PhysRevD.63.054019.

[28] **CMS** Collaboration, S. Chatrchyan et al., "Measurements of differential jet cross sections in proton-proton collisions at $\sqrt{s} = 7$ TeV with the CMS detector," *Phys. Rev. D* **87** (2013) 112002, arXiv:1212.6660. doi:10.1103/PhysRevD.87.112002.

[29] **CMS** Collaboration, V. Khachatryan et al., "Constraints on parton distribution functions and extraction of the strong coupling constant from the inclusive jet cross section in pp collisions at $\sqrt{s} = 7$ TeV," *Eur. Phys. J. C* **75** (2015) 288, arXiv:1410.6765. doi:10.1140/epjc/s10052-015-3499-1.

[30] S. Frixione, P. Nason, and C. Oleari, "Matching NLO QCD computations with Parton Shower simulations: the POWHEG method," *JHEP* **11** (2007) 070, arXiv:0709.2092. doi:10.1088/1126-6708/2007/11/070.

[31] T. Sjöstrand, S. Mrenna, and P. Z. Skands, "PYTHIA 6.4 Physics and Manual," *JHEP* **05** (2006) 026, arXiv:hep-ph/0603175. doi:10.1088/1126-6708/2006/05/026.

[32] M. Bähr, S. Gieseke, M. Gigg, D. Grellscheid, K. Hamilton, O. Latunde-Dada, S. Plätzer, P. Richardson, M. H. Seymour, A. Sherstnev, and B. R. Webber, "Herwig++ Physics and Manual," *Eur. Phys. J. C* **58** (2008) 639, arXiv:0803.0883. doi:10.1140/epjc/s10052-008-0798-9.

[33] J. R. Andersen et al., "Les Houches 2013: Physics at TeV Colliders: Standard Model Working Group Report," arXiv:1405.1067.

[34] Z. Nagy, "Three jet cross-sections in hadron hadron collisions at next-to-leading order," *Phys. Rev. Lett.* **88** (2002) 122003, arXiv:hep-ph/0110315. doi:10.1103/PhysRevLett.88.122003.

[35] Z. Nagy and Z. Trocsanyi, "Multi-jet cross sections in deep inelastic scattering at next-to-leading order," *Phys. Rev. Lett.* **87** (2001) 082001, arXiv:hep-ph/0104315. doi:10.1103/PhysRevLett.87.082001.

[36] T. Kluge, K. Rabbertz, and M. Wobisch, "fastNLO: Fast pQCD calculations for PDF fits," in *14th International Workshop on Deep-Inelastic Scattering (DIS 2006)*, p. 483. Tsukuba, Japan, 20-24 Apr 2006, 2006. arXiv:hep-ph/0609285.

[37] A. Buckley, J. Ferrando, S. Lloyd, K. Nordstrom, B. Page, et al., "LHAPDF6: parton density access in the LHC precision era," arXiv:1412.7420.

[38] D. Britzger, K. Rabbertz, D. Savoiu, G. Sieber, et al., "Alpos: An object-oriented data to theory comparison and fitting framework." https://ekptrac.physik.uni-karlsruhe.de/trac/Alpos, 2014–2016. SVN revision 209.

[39] B. Schmidt and M. Steinhauser, "CRunDec: a C++ package for running and decoupling of the strong coupling and quark masses," *Comput. Phys. Commun.* **183** (2012) 1845, arXiv:1201.6149. doi:10.1016/j.cpc.2012.03.023.

[40] R. Brun and F. Rademakers, "ROOT – An Object Oriented Data Analysis Framework," *Nuclear Instruments and Methods in Physics Research A* **389** (1997) 81–86.

[41] J. Currie, E. W. N. Glover, and J. Pires, "NNLO QCD predictions for single jet inclusive production at the LHC," arXiv:1611.01460.